Original article

Nuclear Medicine Communications

Development of positron emission tomography imaging by ^{64}Cu-labeled Fab for detecting ERC/mesothelin in a mesothelioma mouse model

Chisato Yoshida[a,c], Chizuru Sogawa[a], Atsushi B. Tsuji[a], Hitomi Sudo[a,d], Aya Sugyo[a], Tomoya Uehara[c], Okio Hino[d], Yukie Yoshii[e], Yasuhisa Fujibayashi[e], Toshimitsu Fukumura[b], Mitsuru Koizumi[a], Yasushi Arano[c] and Tsuneo Saga[a]

Background **Malignant mesothelioma is a highly aggressive form of cancer. Curative surgery is the only effective therapy for mesothelioma, and therefore early diagnosis is important. However, early diagnosis is difficult using current diagnostic imaging techniques, and a new imaging method for early diagnosis is urgently required. We evaluated the affinity of radiolabeled monoclonal antibodies to the C-terminal fragment of ERC/mesothelin for this purpose.**

Methods **^{111}In-labeled or ^{125}I-labeled IgG against C-terminal fragment of ERC and its Fab fragment were evaluated *in vitro* by cell binding, competitive inhibition, and cellular internalization assays, and *in vivo* by biodistribution in mice bearing ERC-expressing tumors. Next, the Fab fragment was labeled with the positron emitter ^{64}Cu and evaluated by positron emission tomography (PET).**

Results **Radiolabeled IgG and Fab showed specific binding to ERC-expressing mesothelioma cells with high affinity. Both radiolabeled IgG and Fab internalized into cells after binding to ERC on the cell surface. ^{111}In-labeled IgG accumulated in ERC-expressing tumors and resulted in a moderate tumor-to-blood ratio at 4 days after injection. Furthermore, PET using ^{64}Cu-labeled Fab visualized the tumor at 6 h after injection.**

Conclusion **^{64}Cu-labeled Fab can be useful for ERC-specific PET imaging, and can thus facilitate improved diagnosis of patients with early-stage mesothelioma. *Nucl Med Commun* 00:000–000 © 2010 Wolters Kluwer Health | Lippincott Williams & Wilkins.**

Nuclear Medicine Communications 2010, 00:000–000

Keywords: antibody, ERC/mesothelin, mesothelioma, positron emission tomography

[a]Diagnostic Imaging Group, [b]Molecular Probe Group, Molecular Imaging Center, National Institute of Radiological Sciences, Anagawa, Inage-ku, [c]Department of Molecular Imaging and Radiotherapy, Graduate School of Pharmaceutical Sciences, Chiba University, Inohana, Chuo-ku, Chiba, [d]Department of Pathology and Oncology, Juntendo University School of Medicine, Hongo, Bunkyo-ku, Tokyo and [e]Biomedical Imaging Research Center, University of Fukui, Yoshida, Fukui, Japan

Correspondence to Dr Atsushi B. Tsuji, PhD, Diagnostic Imaging Group, Molecular Imaging Center, National Institute of Radiological Sciences, 4-9-1 Anagawa, Inage-ku, Chiba 263-8555, Japan
Tel: +81 43 206 4643; fax: +81 43 206 4138; e-mail: a_tsuji@nirs.go.jp

Chisato Yoshida and Chizuru Sogawa contributed equally to this study

Received 25 September 2009 **Revised** 1 December 2009
Accepted 10 December 2009

Introduction

Malignant mesothelioma is a highly aggressive form of cancer arising from the serosal surfaces of the pleura, peritoneum, and pericardium [1,2]. Approximately 75% of all cases involve the pleura, whereas the remaining 25% involve the peritoneum or pericardium. Mesothelioma is associated with past asbestos exposure, and has a latency of 30–40 years. The three major subtypes of mesothelioma are epithelioid (50–70% of all cases), sarcomatoid (7–20%), and mixed/biphasic (20–30%). This type of tumor was once rare, but the incidence is expected to increase worldwide over the next several decades as a result of widespread asbestos exposure, both occupational and environmental, in many countries [1–4].

Current treatment includes some form of surgery, which may be combined with chemotherapy and/or radiation. However, the prognosis of patients with this multimodality therapy remains poor [1,2]. Survival depends on stage, histological subtype, patient age, sex, and various other factors. Sugarbaker *et al.* [5] reported median survival rates of 25, 20, and 16 months for patients with stage I, II, and III of the disease, respectively. This finding indicates that early diagnosis is important in improving prognosis. However, early diagnosis is difficult using current diagnostic imaging techniques. The development of a new imaging method for the early diagnosis of mesothelioma is urgently required.

ERC/mesothelin is a 71 kDa cell surface antigen and is present on mesothelium, mesotheliomas, and ovarian cancers. This protein is physiologically cleaved by furin-like proteases into a 40 kDa C-terminal fragment (C-ERC) that remains membrane-bound and a 31 kDa N-terminal fragment (N-ERC) that is secreted into the bloodstream [6]. Recently, we developed new monoclonal antibodies against C-ERCs and N-ERCs [6,7] and reported that serum levels of N-ERC of patients with

0143-3636 © 2010 Wolters Kluwer Health | Lippincott Williams & Wilkins

DOI: 10.1097/MNM.0b013e328336733d

epithelioid mesothelioma were higher than those with other diseases [8]. A sensitive serum N-ERC assay applied in a population with a history of asbestos exposure is expected to detect patients with early-stage disease. Image-guided biopsy of such patients is thought to facilitate definitive diagnosis at early stages of disease. This is carried out using a noninvasive imaging method for detecting C-ERC, in which radiolabeled antibody is expected to play an important role. Although antibodies against C-ERC, ^{111}In-labeled IgG [9] and ^{111}In-labeled tetravalent scFv [10], have previously been evaluated by other research groups, the major aim of such studies was the development of therapeutic agents. Consequently, the same research groups have recently conducted clinical trials for the treatment of ERC-expressing tumors [11]. Positron emission tomography (PET), with higher sensitivity and greater quantification ability than single-photon emission computed tomography, seems to be suitable for the detection of ERC expression in early-stage mesothelioma.

In this study, we performed in-vitro and in-vivo investigations of ^{111}In-labeled or ^{125}I-labeled anti-C-ERC IgG and its Fab fragment to evaluate their use as an imaging probe for detecting ERC expression. To apply this Fab fragment to PET imaging, we labeled Fab with positron-emitting ^{64}Cu and monitored in-vivo distribution through PET imaging of human mesothelioma xenografts in nude mice.

Methods

Cell culture

Human mesothelioma cell lines, H226 and 211H, were obtained from American Type Culture Collection (Manassas, Virginia, USA). These cell lines were maintained in RPMI1640 (Sigma, St Louis, Missouri, USA) containing 5% fetal bovine serum in a humidified incubator maintained at 37°C with 5% CO_2. ERC was highly expressed in H226 cells and slightly in 211H cells [12].

Chelate conjugation and radiolabeling with ^{111}In, ^{125}I, and ^{64}Cu

Anti-C-ERC mouse monoclonal IgG_{2a} (22A31) [7] and its Fab fragment were conjugated with *N*-[(*R*)-2-amino-3-(*p*-isothiocyanato-phenyl)propyl]-*trans*-(*S*,*S*)-cyclohexane-1,2-diamine-*N*,*N*,*N*′,*N*″,*N*‴-penta-acetic acid [*p*-SCN-Bz-CHX-A″-DTPA (DTPA), Macrocyclics, Dallas, Texas, USA] or 2-(4-isothiocyanatobenzyl)-1,4,7,10-tetra-azacyclododecane-1,4,7,10-tetra-acetic acid [*p*-SCN-Bz-DOTA (DOTA), Macrocyclics]. Either the IgG or Fab antibody was incubated with DTPA or DOTA in 0.05 mol/l borate buffer (pH 8.5) for 16 h at 37°C. The conjugation ratio of DTPA and DOTA to antibody was estimated to be 1.7–2.1. ^{111}In chloride (Nihon Medi-Physics, Tokyo, Japan) prepared in 1 mol/l of acetate buffer (pH 6.0) was incubated with the DTPA-conjugated or DOTA-conjugated antibody for 30 min at room temperature or 37°C, respectively. The labeling efficiency of ^{111}In-labeled or ^{125}I-labeled antibodies was determined by cellulose acetate electrophoresis. The radiolabeled antibodies were purified by a Sephadex G-50 (GE Healthcare, Little Chalfont, UK) column. The specific activity of ^{111}In-DTPA-IgG and ^{111}In-DTPA-Fab was approximately 50 and 55 kBq/μg, respectively. ^{64}Cu chloride was produced by a cyclotron in our institute according to a previously reported method [13]. The DOTA-conjugated Fab was incubated with 37 MBq of ^{64}Cu in 0.1 mol/l ammonium citrate (pH 5.5) for 1 h at 37°C. The ^{64}Cu-DOTA-Fab was purified by a Sephadex G-50 column. Labeling efficiency was determined by thin-layer chromatography using 80% methanol as the mobile phase, and the radiolabeled antibodies were purified by a Sephadex G-50. The specific activity of ^{64}Cu-DOTA-Fab was 74–140 kBq/μg. Radioiodination was performed using the chloramine-T method [14]. The specific activity of ^{125}I-IgG and ^{125}I-Fab was approximately 850 and 740 kBq/μg, respectively. After radiolabeling, the radiochemical purity of the antibody was examined through high-performance liquid chromatography on a 5Diol-300-II column (Nakarai, Kyoto, Japan) and an isocratic mobile phase of 100 mmol/l of phosphate buffer (pH 6.8) at a flow rate of 1 ml/min.

In-vitro assay

In a cell-binding assay, serially diluted H226 cells (5×10^6 to 2×10^4 cells) or 211H cells (1×10^7 to $\times 10^6$) in phosphate-buffered saline (PBS) were incubated with the radiolabeled antibody (20 kcpm) for 1 h on ice. The cells were then centrifuged and washed twice with PBS. The radioactivity bound to the cells was counted using an auto-well gamma counter (ALOKA, Tokyo, Japan). The immunoreactivity of radiolabeled antibodies was measured according to the method of Lindmo *et al.* [15]. In a competitive inhibition assay, the radiolabeled antibody (20 kcpm) was incubated with 2×10^6 H226 cells in the presence of varying concentrations of the unlabeled antibody (0, 0.05, 0.1, 0.5, 1, 5, and 10 μg/ml) for 1 h on ice. The cells were then centrifuged and washed twice with PBS. The radioactivity bound to the cells was counted. The data were analyzed by GraphPad Prism software (Graphpad Software, La Jolla, California, USA) to determine the dissociation constants. In an internalization assay, H226 cells (2×10^6) in a culture medium were preincubated with radiolabeled antibody (20 kcpm) for 1 h at 4°C. The cells were washed once with a culture medium and collected by centrifugation. The collected cells were further cultured at 37°C or on ice in a fresh medium without radiolabeled antibodies. At various time points, the supernatant and the cells were separated by centrifugation. The supernatant was added with 10% trichloroacetic acid (Sigma) for 15 min on ice and then separated by centrifugation to determine the nonprotein-bound fraction (supernatant) and protein-bound fraction (pellet). The cells were washed with acidic buffer

[0.05 mol/l of glycine HCl (pH 2.8) and 0.1 mol/l of NaCl] for 15 min at room temperature, and were then separated by centrifugation to determine both the membrane-bound fraction (supernatant) and internalized fraction (pellet).

Biodistribution of ^{111}In-labeled or ^{125}I-labeled antibody in mouse models

Female BALB/c-nu/nu mice (5 weeks old, CLEA Japan, Tokyo, Japan) were inoculated with 4×10^6 H226 and 2×10^6 211H cells subcutaneously in the left and right thighs, respectively. As 211H cells grow faster than H226 cells in mice ($\sim$15 days difference), the inoculation day of each cell line was adjusted to ensure that the tumor xenografts were of equal size. The experiments were performed when the xenografted tumors reached a diameter of approximately 10 mm. For the biodistribution experiments, mice bearing H226 and 211H tumors were intravenously injected with a mixture of ^{111}In-labeled or ^{125}I-labeled antibodies (IgG or Fab, 37 kBq each). The injection protein dose was adjusted to 5 μg per mouse by adding the unlabeled antibody. At 24, 48, and 96 h after injection of IgG or at 1, 6, and 12 h after injection of Fab, the groups of mice (n=5 each) were killed and blood was obtained from the heart. The tumor and major organs were removed and weighed. Radioactivity was measured using the gamma counter. The data were expressed as percentage of injected dose per gram of tissues (% ID/g) normalized to a mouse with a body weight of 20 g. The statistical differences in tumor uptake were compared between H226 and 211H tumors using the Student's t-test (two-tailed). The experimental protocol was approved by the Institutional Animal Care and Use Committee of our institute, and all animal experiments were performed in accordance with the Institutional guidelines on animal care and handling.

Biodistribution and PET imaging of ^{64}Cu-DOTA-Fab

Mice bearing H226 tumor were injected with ^{64}Cu-DOTA-Fab (37 kBq in 5 μg protein). At 1, 6, and 12 h after injection of Fab, the groups of mice (n=5 each) were killed and the biodistribution was determined as described earlier. The statistical differences in tumor uptake were compared between ^{64}Cu-DOTA-Fab and ^{111}In-DTPA-Fab tumors using the Student's t-test (two-tailed). For PET experiments, a mouse bearing a H226 tumor was injected in the tail vein with approximately 4 MBq of ^{64}Cu-DOTA-Fab. At 1, 6, and 15 h post injection, the mouse was anesthetized using isoflurane and imaged using a small animal PET scanner (Inveon, Siemens Medical Solutions, Malvern, Pennsylvania, USA). The acquisition time was 30 (at 1 and 6 h) or 60 min (at 15 h), and the images were reconstructed using a three-dimensional maximum a posteriori (18 iterations with 16 subsets, β=0.2 resolution) without attenuation correction.

Results

In-vitro characterization of ^{111}In-labeled or ^{125}I-labeled IgGs and Fabs

We conducted cell binding assays with H226 (high ERC expression) or 211H (low ERC expression) cells with ^{111}In-labeled or ^{125}I-labeled IgG and Fab. Binding of 5×10^6 H226 cells to ^{111}In-DTPA-IgG, ^{125}I-IgG, ^{111}In-DTPA-Fab, and ^{125}I-Fab was 77.5, 64.0, 63.8, and 63.3%, respectively (Figs 1a and 2a), and that of 5×10^6 211H cells to ^{125}I-IgG and ^{125}I-Fab was 30.5, and 28.7%, respectively (data not shown). The immunoreactive fractions of ^{111}In-DTPA-IgG, ^{125}I-IgG, ^{111}In-DTPA-Fab, and ^{125}I-Fab were calculated as 87, 70, 82, and 64%, respectively. The results of the competitive inhibition assay revealed the dissociation constants for ^{111}In-DTPA-IgG, ^{125}I-IgG, ^{111}In-DTPA-Fab, and ^{125}I-Fab to be 7.8, 4.3, 5.0, and 8.0 nmol/l, respectively, and the number of binding sites for ^{111}In-DTPA-IgG and ^{125}I-IgG to be 6.6×10^4 and 7.5×10^4 per H226 cell, respectively (Figs 1b and 2b). We examined the temporal change in radioactivity localization of ^{111}In-labeled or ^{125}I-labeled IgG and Fab in H226 cells (Figs 1c, d and 2c, d). The cell membrane-bound fraction of ^{111}In-DTPA-IgG and ^{125}I-IgG rapidly decreased over time, and 23.6% of ^{111}In-DTPA-IgG and 16.1% of ^{125}I-IgG internalized after incubation at maximum (Fig. 1c and d). The nonprotein-bound fraction of ^{125}I-IgG in the culture medium increased over time (Fig. 1d). The internalization assay for ^{111}In-DTPA-Fab and ^{125}I-Fab showed that the internalized fraction of ^{111}In-DTPA-Fab and ^{125}I-Fab slightly increased (Fig. 2c and d), and the nonprotein-bound fraction of ^{125}I-Fab in the medium increased (Fig. 2d) similar to that of IgG. The protein-bound fraction of radiolabeled Fabs in the medium increased more than that of radiolabeled IgG (Figs 1c, d and 2c, d). When cells were incubated on ice, the membrane-bound fraction did not change and internalization was not observed for at least 3 h (data not shown).

Biodistribution of ^{111}In-labeled or ^{125}I-labeled IgGs and Fabs

The biodistribution experiments using ^{111}In-DTPA-IgG, ^{125}I-IgG, ^{111}In-DTPA-Fab, and ^{125}I-Fab were performed in nude mice bearing H226 and 211H tumors (Figs 3 and 4). ^{111}In-DTPA-IgG accumulated in H226 tumors at 5.3 ± 0.9% ID/g after 24 h and reached a peak value of 5.8 ± 0.5% ID/g at 48 h, while the tumor uptake of ^{125}I-IgG (2.5 ± 0.6% ID/g at 24 h) was lower than that for ^{111}In-DTPA-IgG and decreased over time (Fig. 3a and b). The uptake of ^{111}In-DTPA-IgG by 211H tumors (4.8 ± 1.6% ID/g at 24 h), which overall expressed lower amounts of ERC *in vitro* than H226 tumors, was comparable to that by H226 tumors at 24 h but decreased thereafter (Fig. 3a). The uptake of ^{125}I-IgG by 211H tumors also decreased over time (Fig. 3b), similar to that by H226 tumors. The uptake of ^{111}In-DTPA-IgG by H226 tumors at 96 h was significantly higher than that by

Fig. 1

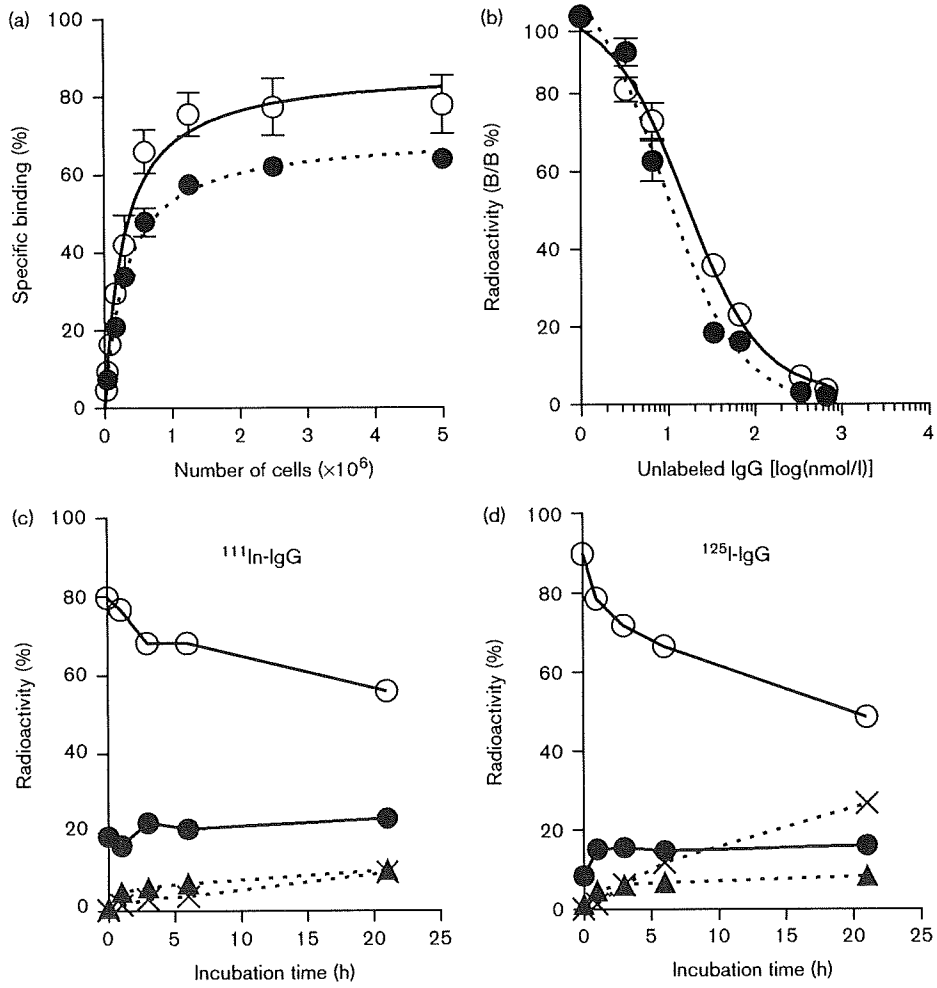

In-vitro assay for radiolabeled anti-ERC IgG in H226 cells. (a) Cell binding assay for radiolabeled IgG (open circles, ^{111}In-DTPA-IgG; closed circles, ^{125}I-IgG). Serially diluted cells were incubated with radiolabeled IgG for 1 h on ice. Cells were washed and radioactivity was counted. (b) Competitive inhibition assay for radiolabeled IgG (open circles, ^{111}In-DTPA-IgG; closed circles, ^{125}I-IgG). Radiolabeled IgG was incubated with cells in the presence of different concentrations of unlabeled IgG for 1 h on ice. Cells were washed and radioactivity was counted. Internalization assay for ^{111}In-DTPA-IgG (c) and ^{125}I-IgG (d). The radioactivity at time 0 shows the value after 1 h of preincubation with H226 cells on ice. Changes in % of total radioactivity for each fraction are plotted against incubation time at 37°C (closed circles, internalized fraction; open circles, membrane-bound fraction; closed triangles, protein-bound fraction in the culture medium, cross marks, nonprotein-bound fraction in the culture medium).

211H tumors ($P < 0.05$, Fig. 3a). The uptake of ^{111}In-DTPA-IgG by major organs was consistent with that of radiolabeled IgGs compared with other antibody–antigen combinations, as reported in earlier studies [14,16], except for the liver and kidney. The tumor-to-blood ratio of ^{111}In-DTPA-IgG was 0.8 and 0.7 at 24 h and increased to 2.4 and 1.7 at 96 h in H226 tumors and 211H tumors, respectively.

The uptake of ^{111}In-DTPA-Fab by H226 tumors was 1.6 ± 0.6, 2.1 ± 0.6, and 1.8 ± 0.2% ID/g at 1, 6, and 12 h, respectively, while that by 211H tumors was 1.2 ± 0.7, 0.9 ± 0.5, and 0.7 ± 0.2% ID/g, respectively (Fig. 4a). The uptake of ^{111}In-DTPA-Fab by H226 tumors at 1 h was similar to that for 211H tumors. However, the uptake by H226 tumors at 6 and 12 h was significantly higher than that in 211H tumors ($P < 0.01$, Fig. 4a). The uptake of ^{125}I-Fab by H226 and 211H tumors was 2.5 ± 0.7 and 2.0 ± 1.1% ID/g at 1 h, respectively, and rapidly decreased over time (Fig. 4b). Consistent with earlier studies assessing Fab labeled with radionuclide [17–20], the uptake of ^{111}In-DTPA-Fab by the kidney was extremely high, reaching a maximum of approximately 95% ID/g (Fig. 4a). The tumor-to-blood ratio of ^{111}In-DTPA-Fab in H226 tumors was 0.2, 1.3, and 2.6 at 1, 6, and 12 h, while that in 211H tumors was 0.1, 0.6, and 1.0, respectively.

Fig. 2

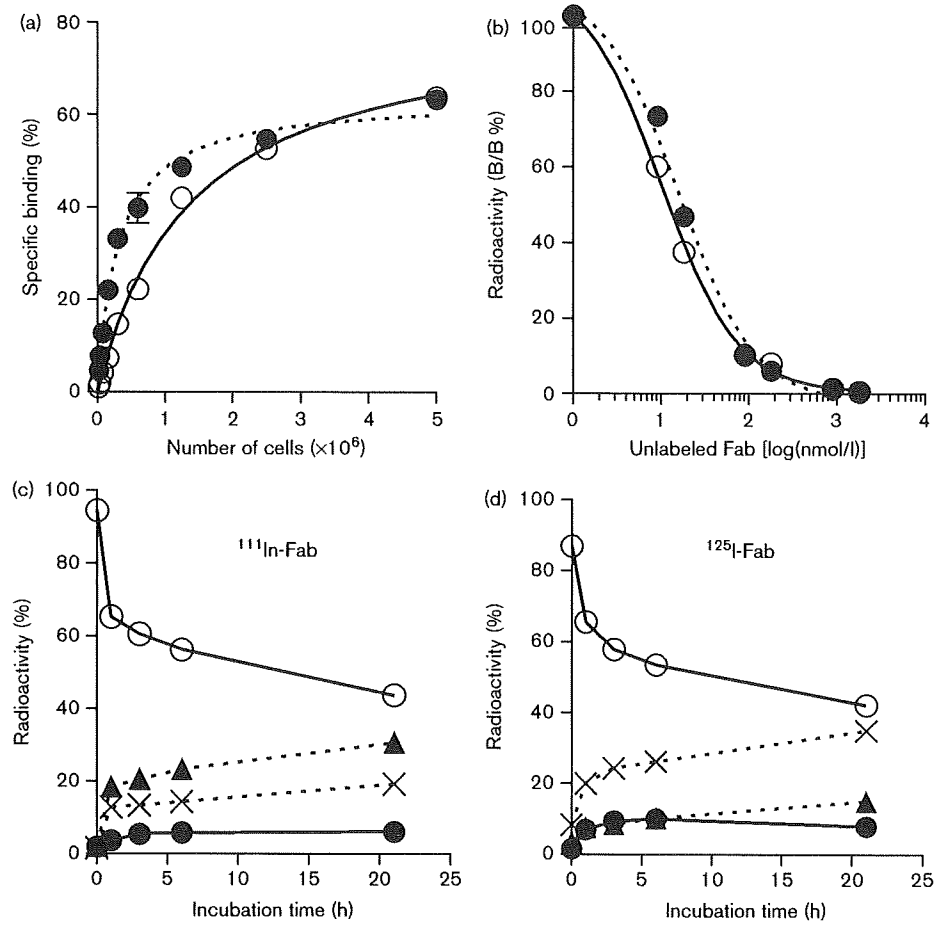

In-vitro assay for radiolabeled anti-ERC Fab in H226 cells. (a) Cell binding assay for radiolabeled IgG (open circles, ^{111}In-DTPA-Fab; closed circles, ^{125}I-Fab). (b) Competitive inhibition assay for radiolabeled Fab (open circles, ^{111}In-DTPA-Fab; closed circles, ^{125}I-Fab). Internalization assay for ^{111}In-DTPA-Fab (c) and ^{125}I-Fab (d). Changes in % of total radioactivity for each fraction are plotted against incubation time at 37°C (closed circles, internalized fraction; open circles, membrane-bound fraction; closed triangles, protein-bound fraction in the culture medium, cross marks, nonprotein-bound fraction in the culture medium).

Cell binding assay, biodistribution, and PET imaging of ^{64}Cu-DOTA-Fab

We conducted a cell-binding assay and biodistribution study of ^{64}Cu-DOTA-Fab similar to those for ^{111}In-labeled or ^{125}I-labeled Fabs. The cell-binding assay showed that binding of ^{64}Cu-DOTA-Fab to H226 cells (80.3% at 5×10^6 H226 cells) was greater than that of ^{111}In-labeled or ^{125}I-labeled Fabs, and an immunoreactive fraction of ^{64}Cu-DOTA-Fab was estimated to be 98% (Fig. 5a). In the biodistribution study, ^{64}Cu-DOTA-Fab accumulated in H226 tumors at 2.0 ± 0.2, 3.1 ± 0.2, and 2.1 ± 0.2% ID/g after 1, 6, and 12 h, respectively (Fig. 5b). These values tended to be higher than those of ^{111}In-DTPA-Fab at all time points, with a significantly higher peak value at 6 h ($P < 0.01$). The renal uptake was 54.0 ± 7.5, 57.7 ± 5.3, and 38.9 ± 2.4% ID/g after 1, 6, and 12 h, respectively; these values are lower than those of ^{111}In-DTPA-Fab. The tumor-to-blood ratio of ^{64}Cu-DOTA-Fab was 0.2, 1.2, and 2.1 after 1, 6, and 12 h, respectively, which were similar to those of ^{111}In-DTPA-Fab.

We performed serial PET imaging of ^{64}Cu-DOTA-Fab in a mouse bearing the H226 tumor at 1, 6, and 15 h after injection (Fig. 5c). The whole body radioactivity was high at 1 h, especially in the kidney, liver, and blood pool. After 6 h or more, the background activity became lower and the H226 tumor was visualized.

Discussion

The prognosis of patients with mesothelioma treated with current therapy remains poor. However, patients diagnosed at an early stage have the potential for prolonged survival. For early-stage diagnosis, image-guided biopsy combined with noninvasive imaging of a

Fig. 3

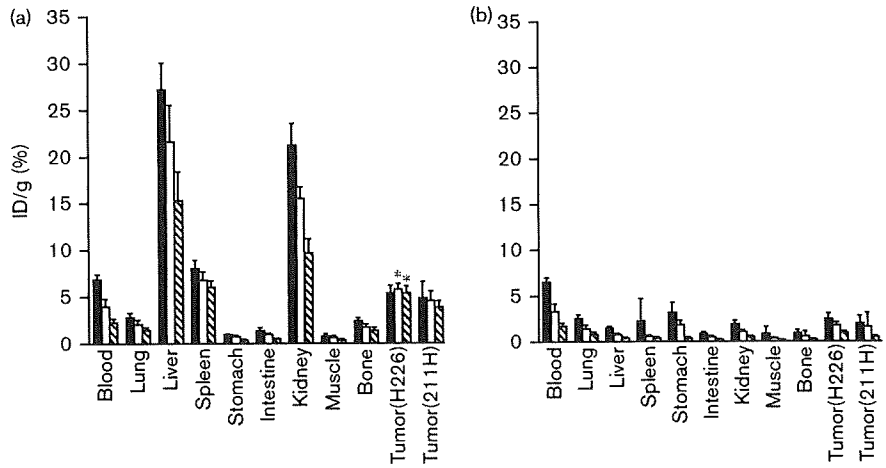

In-vivo biodistribution experiments in nude mice bearing H226 and 211H xenografts of radiolabeled IgGs. Samples were collected and weighed and radioactivity was measured at 24 (black bars), 48 (white bars), and 96 h (diagonal bars) after intravenous injection of 37 kBq each of ^{111}In-DTPA-IgG (a) and ^{125}I-IgG (b). *$P<0.05$ for *t*-tests comparing time-specific uptake of radiolabeled IgGs by H226 and 211H. ID, injected dose.

Fig. 4

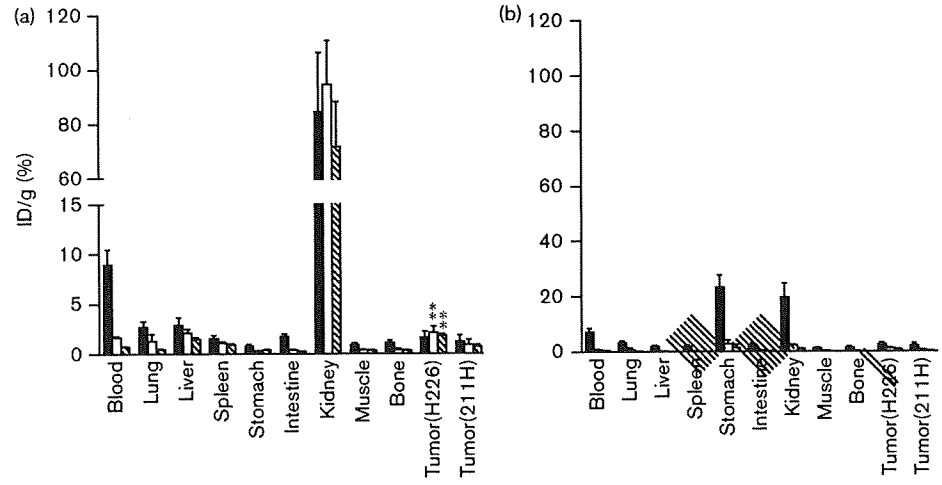

In-vivo biodistribution experiments in nude mice bearing H226 and 211H xenografts of radiolabeled Fabs. Samples were collected and weighed and radioactivity was measured at 1 (black bars), 6 (white bars), and 12 h (diagonal bars) after intravenous injection of 37 kBq each of ^{111}In-DTPA-Fab (a) and ^{125}I-Fab (b). **$P<0.01$ for *t*-tests comparing time-specific uptake of radiolabeled Fabs by H226 and 211H. ID, injected dose.

mesothelioma-specific marker would be useful. ERC is expressed in mesothelioma from an early stage and is thought to be a candidate for marker-specific imaging. In this study, we evaluated the affinity of radiolabeled monoclonal antibodies for C-ERC *in vitro* and *in vivo* for ERC-specific PET imaging.

To evaluate the radiolabeled anti-ERC antibody, we used mesothelioma cell lines and mouse xenograft models with varying degrees of ERC expression. On the basis of our earlier study, we selected the H226 cell line as a model for high ERC expression and the 211H cell line as a model for low ERC expression [12]. In this study, H226 cells showed high in-vitro binding to the anti-ERC antibody, whereas 211H cells showed lower binding. We therefore used mouse xenograft models of these two cell lines to evaluate the in-vivo biodistribution of the anti-C-ERC antibody.

According to the in-vitro study, both ^{111}In-labeled or ^{125}I-labeled IgG showed specific binding to H226 cells with high affinity. The internalization assay showed that ERC was internalized after binding with the antibody. In contrast to ^{125}I, in which free iodine formed after

Fig. 5

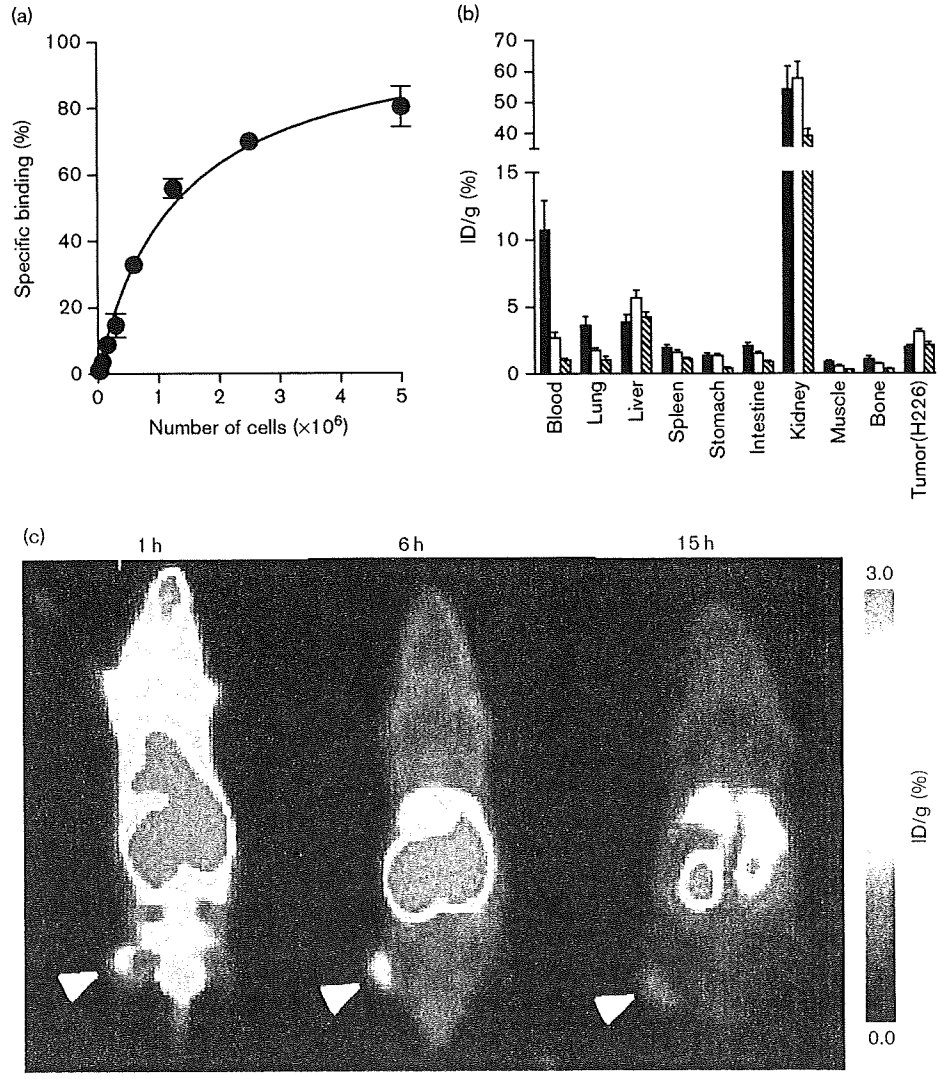

(a) Cell binding assay for ^{64}Cu-DOTA-Fab. (b) Biodistribution in nude mice bearing a H226 xenograft at 1, 6, and 12 h after intravenous injection of 0.37 MBq of ^{64}Cu-DOTA-Fab. (c) Serial positron emission tomography images of a nude mouse bearing a H226 xenografted tumor (arrowhead) at 1, 6, and 15 h after intravenous injection of 4 MBq of ^{64}Cu-DOTA-Fab. ID, injected dose.

internalization and metabolism rapidly exited the cell, ^{111}In radioactivity was retained inside the cells even after internalization. Taken together with earlier studies [14,16], these results suggest that labeling with a metal radionuclide would be suitable for ERC-specific imaging using this antibody. In fact, in-vivo biodistribution studies of ^{111}In-labeled IgG showed higher and more prolonged uptake in H226 tumors than ^{125}I-labeled IgG in mouse xenograft models, confirming the in-vitro findings mentioned above. However, as the clearance of IgG from the blood was very slow, a sufficient tumor-to-blood ratio for imaging could be obtained only at later time points, that is, 96 h.

For the detection of early-stage mesothelioma, high-sensitivity imaging is necessary and PET is the modality of choice that has the potential to meet this requisite. Most positron emitters have relatively short half-lives and are not suitable for PET imaging using IgG. Owing to its long half-life, 4.18 days, ^{124}I can be used for PET imaging with IgG. However, ^{124}I cannot be used for antibodies that undergo internalization and dehalogenation. If a positron-emitting radiometal is used, this technique requires the enhancement of the kinetics of antibodies to match the short half-lives (e.g. 12.7 h for ^{64}Cu). The use of IgG fragments such as Fab and scFv is the most popular way to expedite the clearance of antibodies [21].

Given that downsizing is also advantageous, owing to its effect on reducing the toxicity and radiation burden to the host, we evaluated the radiolabeled Fab fragment. According to the in-vitro assays, radiolabeled Fabs bound specifically to H226 cells, similar to IgGs, and the affinity of radiolabeled Fabs was comparable to that of radiolabeled IgGs. Similar to parental IgG, radiolabeled Fabs also underwent internalization after binding with the antigen. Furthermore, we found a substantial amount of protein-bound fraction in the supernatant, which indicated detached Fab. This result may indicate the decreased binding affinity of the monovalent Fab compared with the divalent IgG, despite the high binding affinity of the Fab. Substantially decreased tumor uptake by ^{64}Cu-labeled or ^{111}In-labeled Fab in the H226 xenografts compared with that by ^{111}In-labeled IgG may reflect the decreased binding affinity of the Fab fragment. Although the tumor-to-blood ratio of radiolabeled Fab did not improve compared with radiolabeled IgG, sufficient tumor-to-blood ratios resulted at earlier times because the clearance of radiolabeled Fab from the blood was rapid. Using ^{64}Cu-labeled Fab, we could obtain a clear delineation of the tumor xenograft at 6 and 15 h after injection. Such results raise the possibility of ERC-specific imaging of patients with early-stage mesothelioma by PET using ^{64}Cu-DOTA-Fab. The uptake of radiolabeled Fabs with metal radionuclides in the kidney was extremely high, which is similar to other Fabs. To counteract this adverse result, the development of a new labeling method with metal radionuclide to decrease renal uptake, such as ^{131}I-iodohippuryl N(ε)-maleoyl-L-lysine, is required [18].

Although we successfully visualized the ERC-expressing xenografted tumor, H226, by ^{64}Cu-DOTA-Fab, tumor uptake seems to be insufficient for clinical application despite high affinity *in vitro*. The H226 cells highly expressed ERC *in vitro*, but the ERC expression of the H226 xenografts was apparently lower than human mesothelioma according to earlier studies [6,12]. Epithelioid mesothelioma in patients forms tubulopapillary architectures and strongly expresses ERC on its surface. However, the H226 tumors used in this study were poorly differentiated compared with typical epithelioid mesothelioma in humans. The discrepancy between in-vitro and in-vivo results in H226 might come from high expression of ERC *in vitro* and low expression *in vivo*. Conversely, the uptake of radiolabeled antibodies in H226 tumors was significantly higher than that in 211H tumors, in which C-ERC expression was not determined by immunohistochemistry [12]. These findings raise the possibility that ^{64}Cu-DOTA-Fab could detect small-sized mesothelioma at an early stage. The use of a model showing higher in-vivo ERC expression may further confirm the potential of this antibody, in addition to improvement in binding affinity. Future research should therefore aim to improve the affinity/avidity of this antibody, for example through the use of divalent scFv [21], and to establish a more clinically relevant tumor model, which forms tubulopapillary architectures and strongly expresses ERC in tumors, to evaluate this antibody before conducting a clinical study.

Conclusion

We evaluated the affinity of radiolabeled IgG and Fab for C-ERC *in vitro* and *in vivo* for use as an imaging probe for mesothelioma-expressing ERC, which is expressed in early-stage mesothelioma. ERC-expressing xenografted tumors could be visualized in nude mice by PET imaging with ^{64}Cu-DOTA-Fab. Our findings suggest that ERC-specific imaging using a positron-emitting radiopharmaceutical ^{64}Cu-DOTA-Fab could be used to diagnose patients with early-stage mesothelioma.

Acknowledgements

We thank Kenichi Odaka for technical advice and help with single-photon emission computed tomography; Hisashi Suzuki, Masami Fukada, and Francisco Lazaro Guerra Gomez for ^{64}Cu production; staff in the Cyclotron Operation section for the cyclotron operation; Yuriko Ogawa for technical assistance; Hidekatsu Wakizaka for the operation and quality control of the PET scanner; and Yoshi-nobu Harada for encouragement.

References

1 Robinson BW, Lake RA. Advances in malignant mesothelioma. *N Engl J Med* 2005; **353**:1591–1603.
2 Tsiouris A, Walesby RK. Malignant pleural mesothelioma: current concepts in treatment. *Nat Clin Pract Oncol* 2007; 4:344–352.
3 Kanazawa N, Ioka A, Tsukuma H, Ajiki W, Oshima A. Incidence and survival of mesothelioma in Osaka, Japan. *Jpn J Clin Oncol* 2006; **36**:254–257.
4 Peto J, Decarli A, La Vecchia C, Levi F, Negri E. The European mesothelioma epidemic. *Br J Cancer* 1999; **79**:666–672.
5 Sugarbaker DJ, Flores RM, Jaklitsch MT, Richards WG, Strauss GM, Corson JM, *et al.* Resection margins, extrapleural nodal status, and cell type determine postoperative long-term survival in trimodality therapy of malignant pleural mesothelioma: results in 183 patients. *J Thorac Cardiovasc Surg* 1999; **117**:54–63. Discussion-5.
6 Maeda M, Hino O. Molecular tumor markers for asbestos-related mesothelioma: serum diagnostic markers. *Pathol Int* 2006; **56**:649–654.
7 Ishikawa K, Segawa T, Hagiwara Y, Maeda M, Abe M, Hino O. Establishment of novel mAb to human ERC/mesothelin useful for study and diagnosis of ERC/mesothelin-expressing cancers. *Pathol Int* 2009; **59**:161–166.
8 Shiomi K, Hagiwara Y, Sonoue K, Segawa T, Miyashita K, Maeda M, *et al.* Sensitive and specific new enzyme-linked immunosorbent assay for N-ERC/mesothelin increases its potential as a useful serum tumor marker for mesothelioma. *Clin Cancer Res* 2008; **14**:1431–1437.
9 Hassan R, Wu C, Brechbiel MW, Margulies I, Kreitman RJ, Pastan I. 111Indium-labeled monoclonal antibody K1: biodistribution study in nude mice bearing a human carcinoma xenograft expressing mesothelin. *Int J Cancer* 1999; **80**:559–563.
10 Sato N, Hassan R, Axworthy DB, Wong KJ, Yu S, Theodore LJ, *et al.* Pretargeted radioimmunotherapy of mesothelin-expressing cancer using a tetravalent single-chain Fv-streptavidin fusion protein. *J Nucl Med* 2005; **46**:1201–1209.
11 Kreitman RJ, Hassan R, Fitzgerald DJ, Pastan I. Phase I trial of continuous infusion anti-mesothelin recombinant immunotoxin SS1P. *Clin Cancer Res* 2009; **15**:5274–5279.
12 Tsuji AB, Sogawa C, Sugyo A, Sudo H, Toyohara J, Koizumi M, *et al.* Comparison of conventional and novel PET tracers for imaging

mesothelioma in nude mice with subcutaneous and intrapleural xenografts. *Nucl Med Biol* 2009; **36**:379–388.
13 McCarthy DW, Shefer RE, Klinkowstein RE, Bass LA, Margeneau WH, Cutler CS, *et al.* Efficient production of high specific activity 64Cu using a biomedical cyclotron. *Nucl Med Biol* 1997; **24**:35–43.
14 Saga T, Sakahara H, Yao Z, Nakamoto Y, Sato N, Hattori N, *et al.* Detection of altered adhesion molecule expression in experimental tumors by a radiolabeled monoclonal antibody. *Jpn J Cancer Res* 1997; **88**:1171–1180.
15 Lindmo T, Boven E, Cuttitta F, Fedorko J, Bunn PA Jr. Determination of the immunoreactive fraction of radiolabeled monoclonal antibodies by linear extrapolation to binding at infinite antigen excess. *J Immunol Methods* 1984; **72**:77–89.
16 Saga T, Endo K, Akiyama T, Sakahara H, Koizumi M, Watanabe Y, *et al.* Scintigraphic detection of overexpressed c-erbB-2 protooncogene products by a class-switched murine anti-c-erbB-2 protein monoclonal antibody. *Cancer Res* 1991; **51**:990–994.
17 Sharkey RM, Goldenberg DM. Perspectives on cancer therapy with radiolabeled monoclonal antibodies. *J Nucl Med* 2005; **46 (Suppl 1)**: 115S–127S.
18 Arano Y, Fujioka Y, Akizawa H, Ono M, Uehara T, Wakisaka K, *et al.* Chemical design of radiolabeled antibody fragments for low renal radioactivity levels. *Cancer Res* 1999; **59**:128–134.
19 Becker WS, Behr TM, Cumme F, Rossler W, Wendler J, Kern PM, *et al.* ^{67}Ga citrate versus ^{99m}Tc-labeled LL2-Fab' (anti-CD22) fragments in the staging of B-cell non-Hodgkin's lymphoma. *Cancer Res* 1995; **55**:5771s–5773s.
20 Uehara T, Koike M, Nakata H, Hanaoka H, Iida Y, Hashimoto K, *et al.* Design, synthesis, and evaluation of [^{188}Re]organorhenium-labeled antibody fragments with renal enzyme-cleavable linkage for low renal radioactivity levels. *Bioconjug Chem* 2007; **18**:190–198.
21 Holliger P, Hudson PJ. Engineered antibody fragments and the rise of single domains. *Nat Biotechnol* 2005; **23**:1126–1136.

YGENO-08182; No. of pages: 7; 4C: 3, 6

Genomics xxx (2010) xxx–xxx

Contents lists available at ScienceDirect

Genomics

journal homepage: www.elsevier.com/locate/ygeno

Knockdown of *COPA*, Identified by Loss-of-Function Screen, Induces Apoptosis and Suppresses Tumor Growth in Mesothelioma Mouse Model

Hitomi Sudo [a,b], Atsushi B. Tsuji [a,*], Aya Sugyo [a], Masakazu Kohda [c], Chizuru Sogawa [a], Chisato Yoshida [a], Yoshi-nobu Harada [a], Okio Hino [b], Tsuneo Saga [a]

[a] Diagnostic Imaging Group, Molecular Imaging Center, National Institute of Radiological Sciences, 4-9-1 Anagawa, Inage-ku, Chiba 263-8555, Japan
[b] Department of Pathology and Oncology, Juntendo University School of Medicine, 2-1-1 Hongo, Bunkyo-ku, Tokyo, 113-8421, Japan
[c] Division of Functional Genomics and Systems Medicine, Research Center for Genomic Medicine, Saitama Medical University, 1397-1 Yamane, Hidaka-shi, Saitama 350-1241, Japan

ARTICLE INFO

Article history:
Received 28 August 2009
Accepted 3 February 2010
Available online xxxx

Keywords:
RNAi
Functional screening
Cell proliferation
Mesothelioma
Apoptosis

ABSTRACT

Malignant mesothelioma is a highly aggressive tumor arising from serosal surfaces of the pleura and is triggered by past exposure to asbestos. Currently, there is no widely accepted treatment for mesothelioma. Development of effective drug treatments for human cancers requires identification of therapeutic molecular targets. We therefore conducted a large-scale functional screening of mesothelioma cells using a genome-wide small interfering RNA library. We determined that knockdown of 39 genes suppressed mesothelioma cell proliferation. At least seven of the 39 genes—*COPA, COPB2, EIF3D, POLR2A, PSMA6, RBM8A,* and *RPL18A*—would be involved in anti-apoptotic function. In particular, the COPA protein was highly expressed in some mesothelioma cell lines but not in a pleural mesothelial cell line. *COPA* knockdown induced apoptosis and suppressed tumor growth in a mesothelioma mouse model. Therefore, *COPA* may have the potential of a therapeutic target and a new diagnostic marker of mesothelioma.

Introduction

Malignant mesothelioma is a highly aggressive tumor arising from the serosal surfaces of the pleura, peritoneum, and pericardium [1,2]. About 75% of all cases involve the pleura, and the remaining involve the peritoneum or pericardium. Mesothelioma is associated with previous asbestos exposure with a latency of 30–40 years. The three main categories of mesothelioma are epithelioid (50–70% of all cases), sarcomatoid (7–20%), and mixed/biphasic (20–30%). This tumor was once rare, but the incidence is expected to increase worldwide over the next several decades as a result of widespread asbestos exposure, both occupational and environmental, in many countries [2–4].

Current treatments include some form of surgery, which may be combined with chemotherapy and/or radiation. However, the prognosis of patients with this multimodality therapy remains poor, with typical post-diagnosis survival being 8–18 months [1,2]. Significantly, traditional chemotherapy has yielded poor response rates (typically <15–20%) [1,2]. Thus, the lack of a highly effective therapeutic regimen for mesothelioma underscores the importance of finding new and more effective treatments.

To develop effective drugs for treatment of human cancer, it is important to identify therapeutic target molecules. Small interfering RNAs (siRNA) have been widely used in mammalian cells to define the functional roles of individual genes, particularly in disease. In addition, the development of whole-genome siRNA libraries and use of high throughput loss-of-function screens have allowed systematic detection of genes required for disease processes such as cancer [5–7]. We previously established a high-throughput screening procedure [8,9] and performed a large-scale screening to identify radiation-susceptible genes [9]. In the present study, we screened potential drug target molecules in mesothelioma cells using the high-throughput screening assay with a genome-wide siRNA library, containing small double-stranded RNAs targeted to more than 8,500 human genes, and conducted *in vitro* and *in vivo* functional analysis of several genes identified by this screening.

Results

Primary screening

The siRNA library used in this study contained 8,589 siRNAs consisting of nine sub-libraries: ion binding, ion channel, kinase, membrane transporter, nucleic acid binding, phosphatase, receptor, transcription factor, and transporter (Table 1) in a 96-well format. We performed primary screening by transfecting each siRNA individually into human malignant mesothelioma cells 211H [10] and measured the remaining viable cells at four days after transfection as determined by a sulforhodamine B-based cell proliferation assay [8,9]. Following gene-specific siRNA transfection, we identified 383 genes for which <50% viable cells remained compared with mock-

* Corresponding author. Fax: +81 43 206 4138.
E-mail address: a_tsuji@nirs.go.jp (A.B. Tsuji).

0888-7543/$ – see front matter © 2010 Elsevier Inc. All rights reserved.
doi:10.1016/j.ygeno.2010.02.002

Please cite this article as: H. Sudo, et al., Knockdown of *COPA*, Identified by Loss-of-Function Screen, Induces Apoptosis and Suppresses Tumor Growth in Mesothelioma Mouse Model, Genomics (2010), doi:10.1016/j.ygeno.2010.02.002

Table 1
Summary of genes in the siRNA library and results of the first screen using MSTO-211H mesothelioma cell line.

Library name	Number of genes in library	Genes showing reduced viability	
		<20%[a]	2-500%[a]
Ion binding	1,479	5	23
Ion channel	349	0	2
Kinase	800	5	24
Membrane Transporter	695	0	12
Nucleic acid binding	1,951	39	117
Phosphatase	599	0	3
Receptor	1,425	16	69
Transcription factor	995	7	36
Transporter	296	6	19
Total	8,589	78	305

[a] % viable cells compared with mock transfected cells.

transfected cells (Table 1 and Supplementary Table 1). Of the 383 genes, 78 showed viability of <20%. These 78 most-effective genes had the following functional distribution: ion binding (5), kinase (5), nucleic acid binding (39), receptor (16), transcription factor (7), and transporter (6) (Table 1 and Supplementary Table 1).

Secondary screening

We synthesized additional siRNAs against the 78 genes identified in the primary screening and built an original sub-library containing 156 siRNAs (two distinct siRNAs for each gene) against these 78 genes in the 96-well format. Knockdown of each gene was achieved by each of two distinct gene-specific siRNAs, and we measured viable cells at 2, 4, and 6 days after transfection. For 39 genes, *COPA, COPB2, EIF3D, POLR2A, PSMA6, RBM8A, RPL18A, OR52I1, RPA1, EIF3C, WEE1, RPL8, RPL3, RPL19, EIF3A, RPS2, RPL6, SF3B1, KISS1R, EIF3I, LSM2, RPL4, RPL21, POLR2F, RPL27A, RPL7, SF3B4, RPL5, RPS18, RPLP1, RPL18, KPNB1, EIF3E, SF3B14, RPL11, EIF3G, RPL35A, RPS17,* and *SNRNP200*, both siRNAs reduced cell viability compared with the negative control (Figs. 1A and B, and Supplementary Fig. 1). For 20 other genes, *TBRG1, DIS3, OR2T27, RPS19, SETD1A, RFX3, PHF5A, EPS8L3, MAX, ASCL2, LCE3A, ZC3H8, C9orf98, WWOX, ITPKA, FCGR3B, NDUFAF2, SCAND3, CAT,* and *RXRG*, only one siRNA reduced cell viability (Supplementary Fig. 1).

Apoptosis assay of mesothelioma cells transfected with siRNAs against seven genes

Based on the greatest negative impact on cell viability of siRNA-mediated knockdown of genes in our screen and their functional categories, we selected seven representative genes, *COPA, COPB2, EIF3D, POLR2A, PSMA6, RBM8A,* and *RPL18A*, for further analysis of their contribution to apoptosis. On treatment with specific siRNAs, the expression of these seven genes was reduced to <10% compared with the negative control, as assessed by real-time RT-PCR (Fig. 1C). We first stained nuclei of knockdown cells with Hoechst 33342 at 48 h after transfection and observed them under the fluorescence microscope. Apoptosis in cell populations transfected with gene-specific siRNAs targeting the seven selected genes apparently increased compared with cells transfected with the negative control siRNA (data not shown). Using flow cytometry, we then measured annexin V-positive apoptotic cells at 8, 24, and 48 h after transfection (Fig. 2). In the negative control, the apoptotic population was not increased at any time point after transfection. At 24 h after transfection, cells transfected with siRNAs targeting five genes, *EIF3D, POLR2A, PSMA6, RBM8A,* and *RPL18A*, contained significantly more apoptotic cells compared with the negative control ($P<0.01$, Fig. 2B), whereas cells transfected with *COPA* and *COPB2* siRNAs did not. At 48 h after transfection, the apoptotic population in all seven of the gene-knockdown cells was significantly increased compared with the negative control ($P<0.01$; Figs. 2A and B). Among cells transfected with the negative control or gene-specific siRNAs, the necrotic population of cells (negative for annexin V and positive for 7-AAD) was not increased at any time point (data not shown).

Functional analysis of COPA in mesothelioma cells

Among these 7 genes, because the *COPA* mRNA has been previously reported to be highly expressed in mesothelioma compared with normal tissues (tumor/normal ratio was 2.19) by microarray experiments [12], we focused on further functional analysis of COPA. To determine whether COPA protein is expressed in mesothelioma, we conducted immunoblotting analysis in four mesothelioma cell lines, 211H, H226, H2052, and H2452, and the pleural mesothelial cell line, MeT-5A. COPA protein was highly expressed in 211H, H2052, and H2452 cells, but not in H226 and MeT-5A cells (Fig. 3A). We examined the ability of *COPA* siRNAs to downregulate *COPA* mRNA in mesothelioma and the pleural mesothelial cell lines by real-time RT-PCR. At 24 h after siRNA-transfection, both siRNAs reduced *COPA* mRNA to <10% in 211H cells compared with the negative control siRNA (Fig. 1C). In H2052 and Met-5A cells, *COPA* mRNAs were reduced to <40% compared with control (Fig. 3B). In H226 and H2452 cells, *COPA* siRNAs were insufficient to reduce *COPA* mRNAs compared with negative control (>60%; Fig. 3B). We then performed cell proliferation assay of *COPA* siRNA-transfected 211H, H2052, and MeT-5A. Both siRNAs (COPAsi1 and COPAsi2) reduced cell viability significantly to <10% (5.4 and 4.6%) and <35% (19.2 and 31.7%) in 211H and H2052, respectively, compared with the negative control, whereas *COPA* siRNA-transfected MeT-5A cells survived >60% (67.1 and 61.2%) compared with control (Fig. 3C).

COPA siRNA treatment in a mesothelioma mouse model

To examine whether *COPA* siRNAs suppress tumor growth in a mesothelioma mouse model, we first conducted treatment experiments with the pretreatment protocol in which 211H cells transfected with *COPA* or negative control siRNAs were subcutaneously injected into nude mice. Fig. 4A shows that negative control siRNA-transfected cells formed tumors that grew linearly with time, whereas 211H cells transfected with both *COPA* siRNAs formed tumors with significant reductions in tumor growth compared with the negative control ($P<0.01$). Second, we conducted a local injection protocol in nude mice bearing 211H xenografts. The untreated 211H cells were subcutaneously inoculated into nude mice, and *COPA* or negative control siRNAs were injected around xenografts twice. The treatment of both *COPA* siRNAs caused significant inhibition in tumor growth compared with the negative control siRNA ($P<0.05$; Fig. 4B).

Fig. 1. Cell viability and gene expression analysis of 211H transfected with seven genes, *COPA, COPB2, EIF3D, POLR2A, PSMA6, RBM8A,* and *RPL18A*. (A) Cell viability of 211H cells transfected with 14 siRNAs against seven genes selected by primary screening shown in Supplementary Table 1 and the negative control siRNA. Cell viability about more 71 genes were shown in Supplementary Fig. 1. Cell viability was measured by sulforhodamine B-based cell proliferation assay at 2, 4, and 6 days after transfection. Data represent mean ± SD from three independent experiments. Open circles represent cells transfected with negative control siRNA, closed squares represent gene-specific siRNA (si1) for each gene, and closed triangles represent gene-specific siRNA (si2) for each gene. (B) Representative sulforhodamine B-stained cells at 2, 4, and 6 days after transfection. Cells transfected with negative control siRNA or gene-specific siRNAs targeting seven genes. (C) Gene expression analysis of 211H cells transfected with siRNAs. The cDNAs were directly synthesized from cells at 24 h after transfection with either negative control siRNA or gene-specific siRNAs targeting seven genes. Gene expression was determined by real-time RT-PCR with TaqMan probes. The expression level of each target gene was normalized to that of 18S ribosomal RNA. Data represent mean and SD from three independent experiments.

Please cite this article as: H. Sudo, et al., Knockdown of *COPA*, Identified by Loss-of-Function Screen, Induces Apoptosis and Suppresses Tumor Growth in Mesothelioma Mouse Model, Genomics (2010), doi:10.1016/j.ygeno.2010.02.002

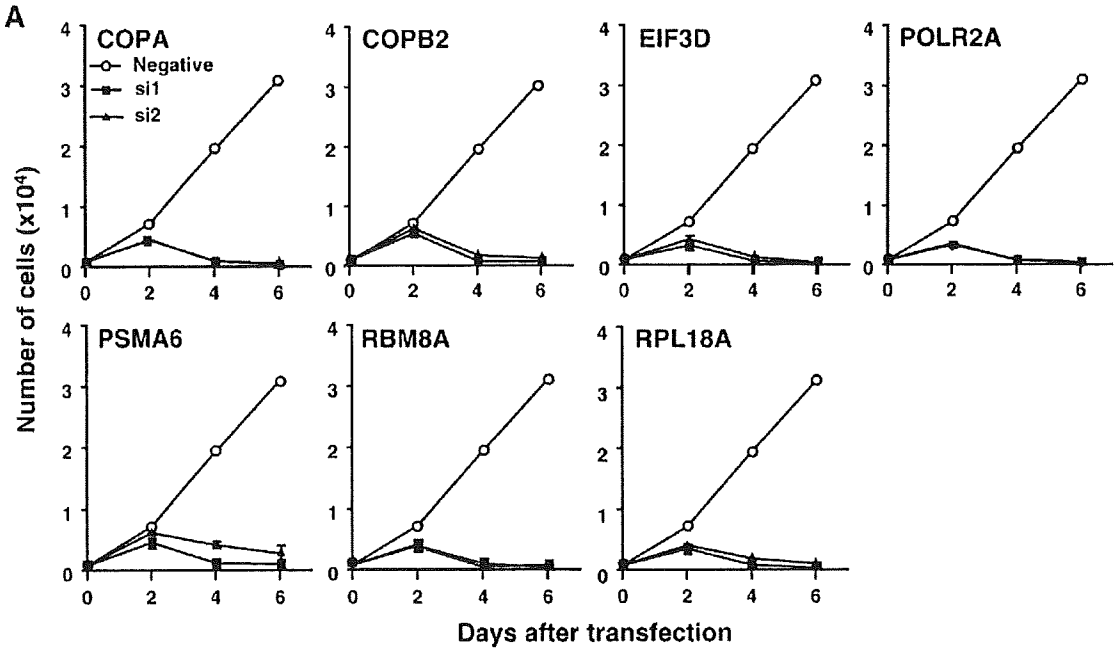

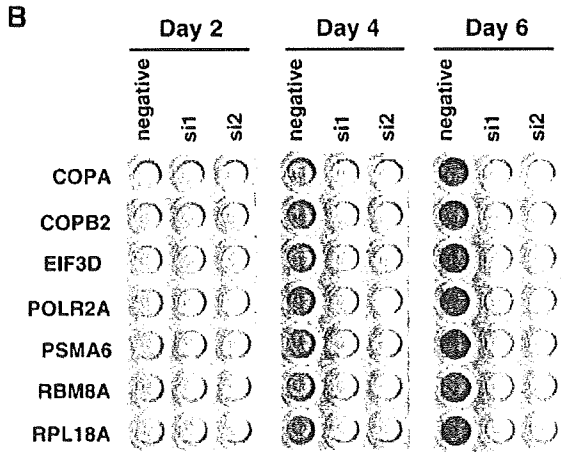

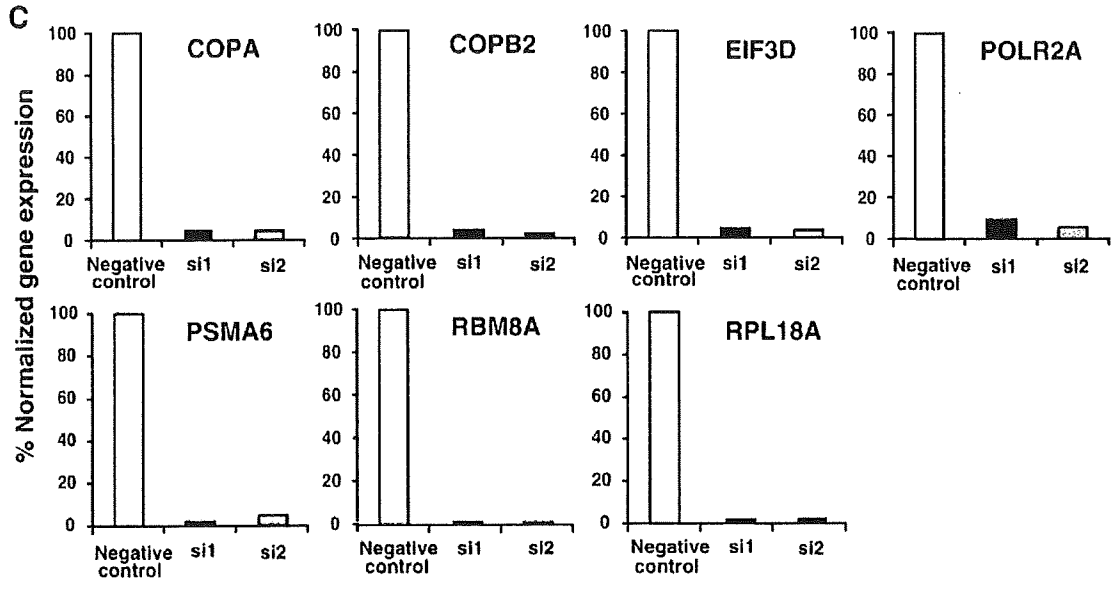

Please cite this article as: H. Sudo, et al., Knockdown of *COPA*, Identified by Loss-of-Function Screen, Induces Apoptosis and Suppresses Tumor Growth in Mesothelioma Mouse Model, Genomics (2010), doi:10.1016/j.ygeno.2010.02.002

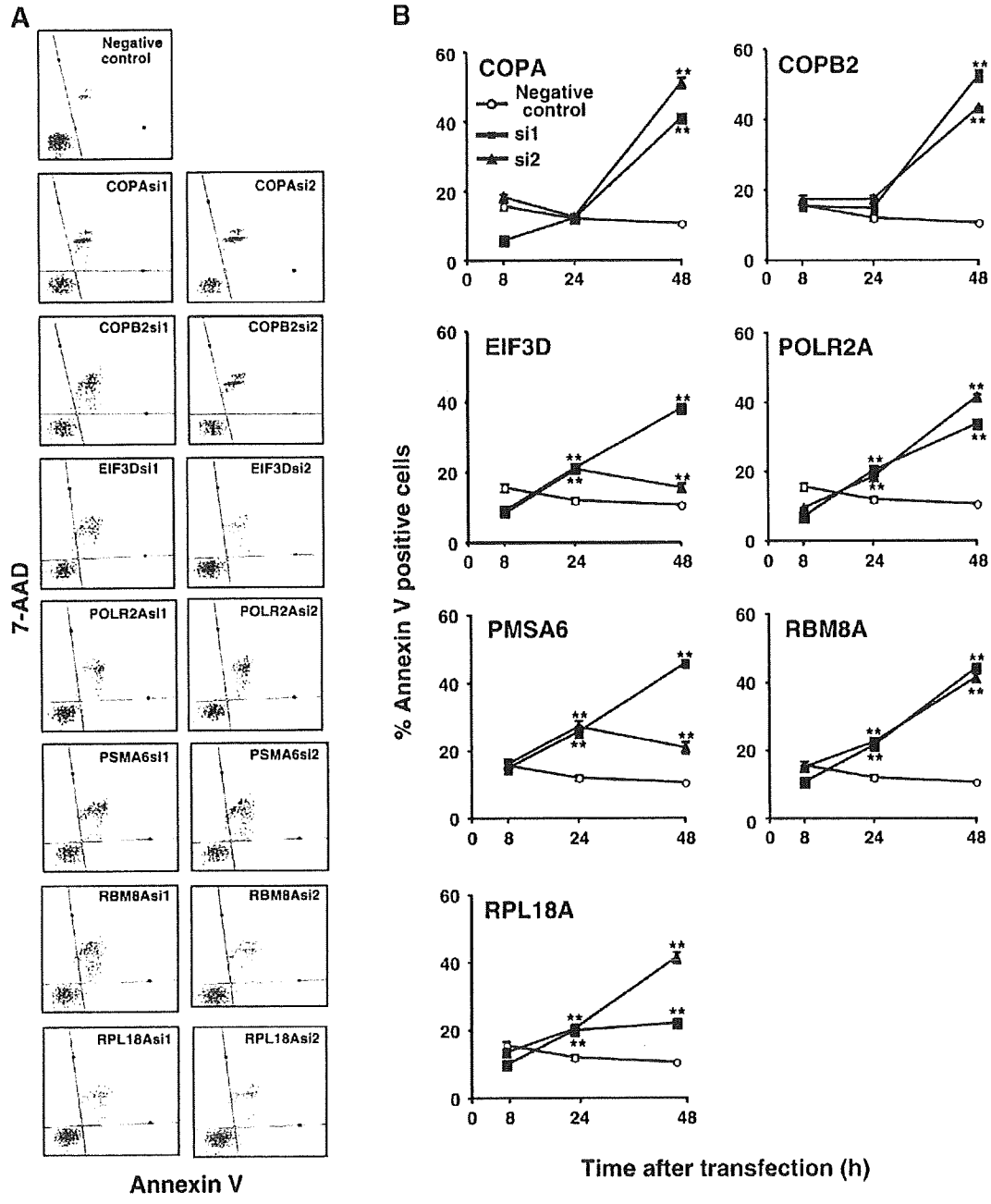

Fig. 2. Apoptotic analysis of 211H cells transfected with seven individual siRNAs against *COPA, COPB2, ELF3D, POLR2A, PSMA6, RBM8A,* and *RPL18A* and stained with annexin V and 7-amino-actinomycin D (7-AAD, DNA staining) at 8, 24, and 48 h after transfection. Living (annexin V negative and 7-AAD negative), necrotic (annexin V negative and 7-AAD positive), and apoptotic (annexin V positive) cells were determined by a Guava PCA system. (A) Representative flow cytometry dot plots at 48 h after transfection. (B) Mean percentage values of apoptotic cell from three independent experiments, as analyzed by ANOVA with the Student–Newman–Keuls method multiple comparison test (vs. negative control, $^{**}P<0.01$). Data are presented as means ± SD from three independent experiments. Open circles represent cells transfected with negative control siRNA, closed squares represent gene-specific siRNA (si1) of each gene, and closed triangles represent gene-specific siRNA (si2) of each gene.

Immunohistochemical staining of 211H xenografted tumors was performed two days after second injection of siRNAs to evaluate apoptosis. We observed a marked increase of apoptotic cells in tumors treated with both *COPA* siRNAs compared with the negative control (Fig. 4C). From quantitative analysis of immunohistochemical staining, both *COPA* siRNAs caused 12- and 10-fold increases of TUNEL-positive cells, respectively, compared with the negative control siRNA ($P<0.01$; Fig. 4D).

Discussion

We report here for the first time a large-scale loss-of-function screening to identify potential drug target molecules for mesothelioma treatments. We conducted a large-scale functional screening of a mesothelioma cell line, 211H, using a genome-wide siRNA library to identify potential drug target molecules. Of siRNAs to 383 genes that reduced mesothelioma cell viability by at least 50%, siRNAs to 78

Please cite this article as: H. Sudo, et al., Knockdown of *COPA*, Identified by Loss-of-Function Screen, Induces Apoptosis and Suppresses Tumor Growth in Mesothelioma Mouse Model, Genomics (2010), doi:10.1016/j.ygeno.2010.02.002

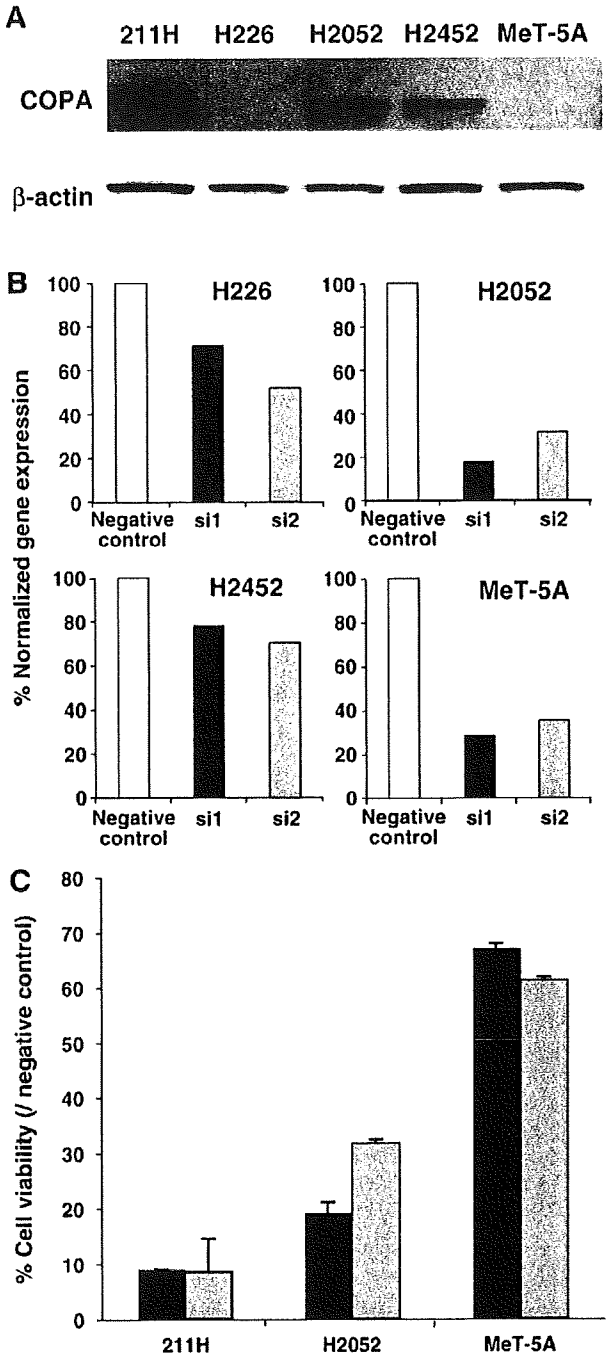

Fig. 3. *COPA* expression in mesothelioma cell lines and cell proliferation of *COPA* siRNA-transfected cells. (A) COPA protein expressions were detected by immunoblot analysis in mesothelioma cell lines (211H, H226, H2052, and H2452) and pleural mesothelial cell line (MET-5A). (B) Expression of *COPA* mRNA was determined by real-time RT-PCR with TaqMan probes. Data represent mean and SD from three independent experiments. (C) Cell proliferation assay of *COPA* siRNA-transfected cells. Data are presented as means and SD from three independent experiments.

genes decreased viability by at least 80%, raising the possibility that these genes regulate cell viability in mesothelioma. To further explore this possibility, we newly synthesized and built an original sub-library containing 156 siRNAs against the above-mentioned 78 genes and assessed the effect of gene silencing on cell viability. Of these 78 genes, we found 39 genes that reduced cell viability at 4 and/or 6 days after transfection with gene-specific siRNAs, suggesting a crucial role for these genes in mesothelioma cell viability and as potential drug targets for treatment. We focused on further functional studies of these 39 genes (mentioned below). For additional 22 genes, cell viability was reduced by one but not both gene-specific siRNAs. This result cannot conclusively establish whether the lack of significant reduction of viable cells resulted from insufficient knockdown in either siRNA or whether the result reflected an off-target effect [7,11]. To clearly identify which of these genes could be associated with cell viability in mesothelioma will require further investigation using additional siRNAs.

Of the 39 genes detected by this screening, almost all cells transfected with siRNAs died at 4 and/or 6 days after transfection. To determine whether apoptosis caused this cell death, we chose seven representative genes, *COPA, COPB2, EIF3D, POLR2A, PSMA6, RBM8A,* and *RPL18A*, based on the greatest negative impact on cell viability of siRNA-mediated knockdown of genes in our screen and their functional categories. According the apoptosis assay of knockdown cells using microscopic and flow cytometric analyses, apoptosis of cell populations targeted with gene-specific siRNAs for each of the seven genes was significantly increased compared with cells with the negative control siRNA. This suggests that these genes can be involved in anti-apoptotic function. Interestingly, *COPA, COPB2, EIF3D,* and *PBM8A* have not been known to be associated with apoptosis. Thus, further investigation of these genes may lead to the elucidation of new molecular mechanisms of apoptosis.

The *COPA* mRNA has been previously reported to be highly expressed in mesothelioma compared with normal tissues [12]. To examine COPA protein expression in mesothelioma cells, we performed immunoblotting analysis for four mesothelioma cell lines (211H, H226, H2052, and H2452) and the pleural mesothelial cell line (MeT-5A). The COPA protein is highly expressed in 211H, H2052, and H2452 cells, but not in H226 and MeT-5A cells. This result suggests that *COPA* could be a new therapeutic target for mesotheliomas that highly express *COPA*. To test this possibility, we conducted cell proliferation assay in 211H, H2052, and MeT-5A cells, in which *COPA* siRNAs were sufficient to reduce *COPA* mRNAs for the assay. *COPA* siRNAs markedly reduced cell viability to <10% and <35% in 211H and H2052 cells, respectively, compared with the negative control, whereas MeT-5A cells survived >60%. We treated mesothelioma mouse models using *COPA* siRNAs with both protocols (pretreatment and local injection) and clearly showed that *COPA* siRNAs suppressed tumor growth and induced apoptosis. The pretreatment protocol was more effective than the local injection protocol. Because the transfection efficiency of mesothelioma cells in dishes is expected to be higher than that in mice, this result was probably due to the transfection efficiency of *COPA* siRNAs. If we could find a small inhibitor molecule of *COPA*, it would help clarify this point and be a potential drug compound for treatment of mesotheliomas that highly express *COPA*.

COPA is one of the seven non-clathrin-coated vesicular coat subunits that form the "coatomer," which plays a role in membrane transport between the endoplasmic reticulum and the Golgi apparatus [13,14]. *COPA* and *COPB2* have a tryptophan-aspartic acid (WD)-repeat motif and belong to a large conserved family of WD proteins found in all eukaryotes and implicated in a variety of functions ranging from signal transduction and transcriptional regulation to cell cycle control and apoptosis [15]. This report and our present results suggest that *COPA* and *COPB2* could play a role not only in membrane transport but also in apoptosis. Thus, further study of *COPA* and *COPB2* might help elucidate the molecular mechanism of apoptosis. *COPA* and *COPB2* have been reported to interact with platelet-derived growth factor β-receptor [16], which is a cell surface tyrosine kinase receptor, binds SH2 domain containing proteins, activates cell growth signaling, and is related to angiogenesis [17,18]. Tumor angiogenesis is a critical step in tumor development through which tumors establish independent nutrient and oxygen supply, consequently enhancing tumor

Please cite this article as: H. Sudo, et al., Knockdown of *COPA*, Identified by Loss-of-Function Screen, Induces Apoptosis and Suppresses Tumor Growth in Mesothelioma Mouse Model, Genomics (2010), doi:10.1016/j.ygeno.2010.02.002

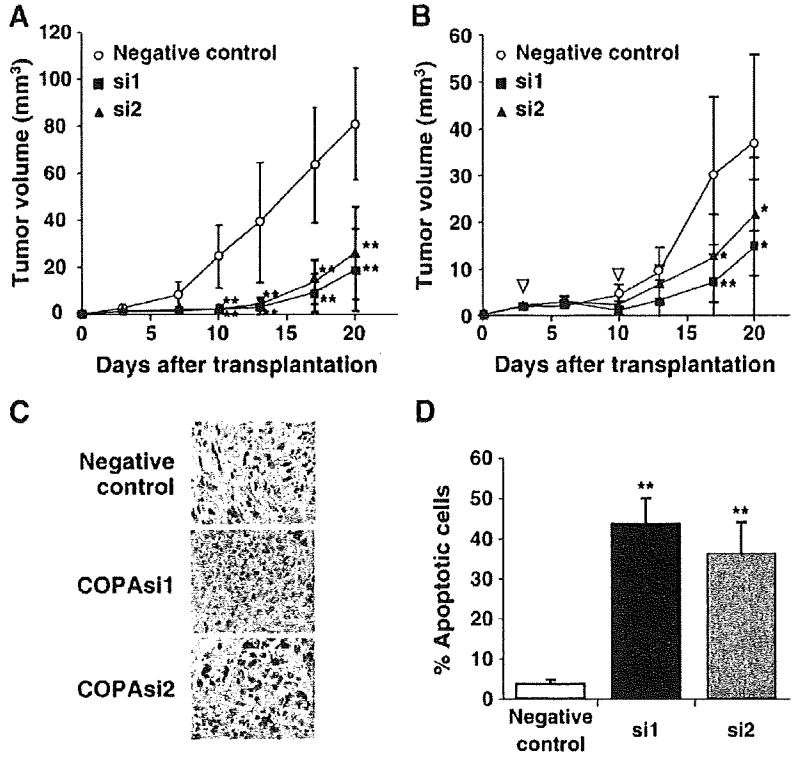

Fig. 4. Therapeutic efficacy of *COPA* siRNA *in vivo*. (A) For the pretreatment protocol, siRNA-transfected 211H cells were injected subcutaneously into nude mice, and tumor diameters were measured at a regular interval for up to 20 days and tumor volume was calculated. Results represent mean ± SD (n = 5) compared with negative control (**P<0.01). Open circles represent cells transfected with negative control siRNA, closed squares represent gene-specific siRNA (si1), and closed triangles represent gene-specific siRNA (si2). (B) For the local injection protocol, 3 and 10 days after inoculation of 211H cells, 10 nmol of *COPA* siRNAs or negative control siRNA was mixed with atelocollagen, and 100 μl of each mixture was injected around tumor. Tumor diameters were measured at a regular interval for up to 20 days and tumor volume was calculated. Results represent the mean ± SD (n = 4 tumors) compared with negative control (*P<0.05, **P<0.01). Open triangles represent siRNA injection. (C) The effect of *COPA* siRNA on apoptosis *in vivo*. Immunohistochemical analysis of 211H tumor xenografts stained with TUNEL (Magnification, 400×, Size bar, 50 μm). (D) The ratio of the apoptotic cells. Data are presented as mean ± SD compared with negative control (**P<0.01).

growth. *COPA* was highly expressed in some mesotheliomas according to our results and the previous report [12]. These findings suggest that *COPA* over-expression could play a role in mesothelioma development through anti-apoptosis and/or angiogenesis. Further studies would be important to explore the correlation between mesothelioma development and potential roles of *COPA* in anti-apoptosis and/or angiogenesis.

In conclusion, we conducted a large-scale functional screening in mesothelioma cells using a genome-wide siRNA library and determined that knockdown of 39 genes suppressed cell proliferation of mesothelioma cells, at least seven of which—*COPA, COPB2, EIF3D, POLR2A, PSMA6, RBM8A,* and *RPL18A*—are associated with an anti-apoptotic function. Functional characterization of these genes and their role in apoptosis pathways may provide clues to the underlying molecular mechanisms of cell death as well as to the development of novel therapeutic agents for mesothelioma. In particular, *COPA* may hold promise for the development of new therapy for malignant mesothelioma that highly express *COPA*.

Materials and methods

Cell culture

We obtained human malignant mesothelioma cell lines, 211H [10], H226, H2052, and H2452, and the human pleural mesothelial cell line MeT-5A from American Type Culture Collections (Manassas, VA). Cells were maintained in RPMI 1640 medium (Sigma, St. Louis, MO) supplemented with 5% fetal calf serum (JRH Biosciences, Lenexa, KS).

SiRNA library

We purchased a human genome-wide siRNA library (siPerfect Library; RNAi Co., Ltd, Tokyo, Japan) containing small double-stranded RNAs against 8,589 human genes. This library consists of nine sub-libraries: ion binding, ion channel, kinase, membrane transporter, nucleic acid binding, phosphatase, receptor, transcription factor, and transporter. We also purchased a negative control siRNA and additional gene-specific siRNAs custom-synthesized by RNAi Co., Ltd.

Cell proliferation assay

We seeded 1.5×10^3 cells in each well of 96-well plates and transfected them with siRNA (5 nM) using Lipofectamine 2000 reagent (Invitrogen, Carlsbad, CA). After 4 days, we performed cell proliferation assay using a sulforhodamine B-based Toxicology Assay kit (Sigma) as reported previously [8,9]. We estimated the numbers of cells based on a standard curve obtained by serial dilutions (10^4 to 625 cells).

Real-time quantitative reverse transcriptase-PCR

We seeded 1.5×10^5 cells in a 3-cm dish and transfected them with siRNA (5 nM). After 24 h, we synthesized first-strand cDNAs from knockdown cells using the FastLane Cell cDNA kit (Qiagen, Hilden, Germany). Predesigned and preoptimized TaqMan probes to detect genes of interest and 18S ribosomal RNA were purchased from Applied Biosystems (Foster City, CA). Real-time reverse transcriptase-PCR (RT-PCR) was performed in triplicate using a Premix Ex Taq

Please cite this article as: H. Sudo, et al., Knockdown of *COPA*, Identified by Loss-of-Function Screen, Induces Apoptosis and Suppresses Tumor Growth in Mesothelioma Mouse Model, Genomics (2010), doi:10.1016/j.ygeno.2010.02.002

reagent (Takara-Bio, Otsu, Japan) on a Mx3000 (Stratagene, La Jolla, CA) real-time PCR instrument. Gene expression levels were normalized to 18S ribosomal RNA expression in each sample.

Apoptosis analysis with Hoechst 33342 staining

We seeded 1.5×10^5 cells in a 6-cm dish and transfected them with siRNAs (10 nM). After 48 h, we added Hoechst 33342 (3 μl; 1 μg/ml; Dojindo Laboratories, Kumamoto, Japan) to the culture medium and incubated the cells for 60 min. The culture medium was then removed and replaced with fresh medium. We observed the stained cells under a fluorescence microscope (Olympus, Tokyo, Japan).

Apoptosis analysis with annexin V staining

We transfected 1.5×10^5 cells with siRNAs (10 nM) and harvested them for 8, 24, and 48 h. The cells were stained with annexin V and 7-amino-actinomycin D (7-AAD) using a Guava PCA Nexin kit (Guava Technologies, Hayward, CA) as described previously [9]. We counted 2,500 events and identified living (annexin V negative, 7-AAD negative), apoptotic (annexin V positive, 7-AAD positive and negative), and necrotic cells (annexin V negative, 7-AAD positive) by a Guava PCA system (Guava Technologies). Data were analyzed by ANOVA with the Student–Newman–Keuls method multiple comparison test.

Immunoblot analysis

We lysed cells in a buffer containing 20 mM Tris-HCl (pH 7.5), 150 mM NaCl, 1 mM EDTA, 1 mM EGTA, 1% Triton X-100, 2.5 mM sodium pyrophosphate, 1 mM β-glycerophosphate, 1 mM Na_3VO_4, 1 μg/ml leupeptin, and 0.2 M 4-(2-Aminoethyl)-benzenesulfonyl fluoride hydrochloride. We estimated the protein concentration using the Quick Start Bradford Protein Assay kit (Bio-Rad, Hercules, CA). Cell lysates (40 μg) were separated by sodium dodecyl sulfate-polyacrylamide gel electrophoresis, transferred to polyvinylidene difluoride membranes using the iBlot Dry Blotting System (Invitrogen), and probed with anti-COPA polyclonal (Abcam, Cambridge, UK) or anti-β-actin monoclonal (Sigma) antibodies. We detected the primary antibodies using horseradish peroxidase-linked goat anti-mouse or anti-rabbit IgG (GE Healthcare, Little Chalfont, UK) and visualized them by the ECL Plus kit (GE Healthcare).

COPA siRNA treatment in mesothelioma mouse models

We obtained female nude mice (BALB/c-nu/nu, 5–6 weeks old) from CLEA Japan (Tokyo, Japan) and maintained them under specific pathogen-free conditions. For a pretreatment protocol, we transfected 211H cells (2×10^6) with COPA-specific (si1 or si2) or control siRNAs, and 24 h later we implanted the cells subcutaneously into the nude mice under ether anesthesia. The size of subcutaneous tumor was measured twice a week using a caliper. Tumor volume was calculated using the following formula: tumor volume (mm^3) = (W × H × D)/2, where W is width, H is height, and D is depth in millimeters. For a local injection protocol, we implanted 2×10^6 of 211H cells subcutaneously into nude mice under ether anesthesia. We treated the tumor-bearing nude mice with 10 nmol of COPA-specific (si1 or si2) or control siRNAs mixed at a ratio of 1:1 in atelocollagen (Koken, Tokyo, Japan) by local injections at 3 and 10 days after subcutaneous tumors had grown to approximately 20 mm^3. We measured the tumor size and calculated the tumor volume. Animal experiments were reviewed and approved by the Institutional Animal Care and Use Committee of our institute.

TUNEL staining of xenografted tumors after treatment

We excised the tumors two days after the last siRNA treatment, fixed them in 10% neutral buffer formalin, and embedded them in paraffin for sectioning and detection of apoptosis. We detected apoptosis by terminal deoxynucleotidyl transferase-mediated deoxyuridine triphosphate biotin nick-end labeling (TUNEL) staining using the ApopTag Plus Peroxidase *In Situ* Apoptosis Detection kit (Chemicon International, Temecula, CA), according to the manufacturer's protocol. Briefly, we stripped nuclear proteins from DNA by incubation in proteinase K for 15 min at room temperature, blocked endogenous peroxidase with 0.3% H_2O_2 for 15 min, and incubated for 10 s with equilibration buffer. The sections were incubated in terminal deoxynucleotidyl transferase enzyme for 1 h at 37 °C. The reaction was terminated by incubation with stop buffer at room temperature. The sections were incubated with anti-digoxigenin conjugate for 30 min, and the reaction was developed with incubation in peroxidase substrate for 5 min. We quantified the TUNEL-stained cells in at least four randomly selected fields at 400× magnification.

Acknowledgments

We thank Sumitaka Hasegawa for technical advices and help, and Yuriko Ogawa for technical assistances. This work was supported in part by a grant from the Ministry of Education, Culture, Sports, Science and Technology of Japan Grant-in Aid for Young Scientists (B) 20790582.

Appendix A. Supplementary data

Supplementary data associated with this article can be found, in the online version, at doi: 10.1016/j.ygeno.2010.02.002.

References

[1] A. Tsiouris, R.K. Walesby, Malignant pleural mesothelioma: current concepts in treatment, Nat. Clin. Pract. Oncol. 4 (2007) 344–352.
[2] B.W. Robinson, R.A. Lake, Advances in malignant mesothelioma, N. Engl. J. Med. 353 (2005) 1591–1603.
[3] N. Kanazawa, A. Ioka, H. Tsukuma, W. Ajiki, A. Oshima, Incidence and survival of mesothelioma in Osaka, Japan, Jpn. J. Clin. Oncol. 36 (2006) 254–257.
[4] J. Peto, A. Decarli, C. La Vecchia, F. Levi, E. Negri, The European mesothelioma epidemic, Br. J. Cancer 79 (1999) 666–672.
[5] K. Berns, et al., A large-scale RNAi screen in human cells identifies new components of the p53 pathway, Nature 428 (2004) 431–437.
[6] J.P. MacKeigan, L.O. Murphy, J. Blenis, Sensitized RNAi screen of human kinases and phosphatases identifies new regulators of apoptosis and chemoresistance, Nat. Cell. Biol. 7 (2005) 591–600.
[7] C.J. Echeverri, N. Perrimon, High-throughput RNAi screening in cultured cells: a user's guide, Nat. Rev. Genet. 7 (2006) 373–384.
[8] A.B. Tsuji, et al., A fast, simple method for screening radiation susceptibility genes by RNA interference, Biochem. Biophys. Res. Commun. 333 (2005) 1370–1377.
[9] H. Sudo, et al., A loss of function screen identifies nine new radiation susceptibility genes, Biochem. Biophys. Res. Commun. 364 (2007) 695–701.
[10] G. Bepler, et al., Characterization of the state of differentiation of six newly established human non-small-cell lung cancer cell lines, Differentiation 37 (1988) 158–171.
[11] A.L. Jackson, et al., Expression profiling reveals off-target gene regulation by RNAi, Nat. Biotechnol. 21 (2003) 635–637.
[12] G.J. Gordon, et al., Identification of novel candidate oncogenes and tumor suppressors in malignant pleural mesothelioma using large-scale transcriptional profiling, Am. J. Pathol. 166 (2005) 1827–1840.
[13] L. Orci, D.J. Palmer, M. Amherdt, J.E. Rothman, Coated vesicle assembly in the Golgi requires only coatomer and ARF proteins from the cytosol, Nature 364 (1993) 732–734.
[14] J.F. Presley, et al., Dissection of COPI and Arf1 dynamics in vivo and role in Golgi membrane transport, Nature 417 (2002) 187–193.
[15] D. Li, R. Roberts, WD-repeat proteins: structure characteristics, biological function, and their involvement in human diseases, Cell. Mol. Life Sci. 58 (2001) 2085–2097.
[16] K. Hansen, L. Ronnstrand, C. Rorsman, U. Hellman, C.H. Heldin, Association of coatomer proteins with the beta-receptor for platelet-derived growth factor, Biochem. Biophys. Res. Commun. 235 (1997) 455–460.
[17] J.F. Rual, et al., Towards a proteome-scale map of the human protein-protein interaction network, Nature 437 (2005) 1173–1178.
[18] D. Anderson, et al., Binding of SH2 domains of phospholipase C gamma 1, GAP, and Src to activated growth factor receptors, Science 250 (1990) 979–982.

Please cite this article as: H. Sudo, et al., Knockdown of *COPA*, Identified by Loss-of-Function Screen, Induces Apoptosis and Suppresses Tumor Growth in Mesothelioma Mouse Model, Genomics (2010), doi:10.1016/j.ygeno.2010.02.002

J Pharmacol Sci 112, 113 – 117 (2010)

Journal of Pharmacological Sciences

Short Communication

Two Non-steroidal Anti-inflammatory Drugs, Niflumic Acid and Diclofenac, Inhibit the Human Glutamate Transporter EAAT1 Through Different Mechanisms

Kanako Takahashi[1,2], Reiko Ishii-Nozawa[1], Kouichi Takeuchi[1], Ken Nakazawa[2], and Kaoru Sato[2,*]

[1]*Department of Clinical Pharmacology, Meiji Pharmaceutical University, Noshio 2-522-1, Kiyose, Tokyo 204-8588, Japan*
[2]*Division of Pharmacology, National Institute of Health Sciences, 1-18-1 Kamiyoga, Setagaya, Tokyo 158-8501, Japan*

Received September 17, 2009; Accepted November 14, 2009

Abstract. We investigated the effects of non-steroidal anti-inflammatory drugs on substrate-induced currents of L-glutamate (L-Glu) transporter EAAT1 expressed in *Xenopus laevis* oocytes. Niflumic acid (NFA) and diclofenac inhibited L-Glu-induced current through EAAT1 in a non-competitive manner. NFA produced a leftward shift in reversal potential (E_{rev}) of L-Glu-induced current and increased current amplitude at the potentials more negative than −100 mV. Diclofenac had no effects on E_{rev} and inhibited the current amplitude to the same extent at all negative potentials. These results indicate that NFA and diclofenac inhibit the L-Glu-induced EAAT1 current via different mechanisms.
[Supplementary methods and Figure: available only at http://dx.doi.org/10.1254/jphs.09260SC]

Keywords: L-glutamate transporter, niflumic acid, diclofenac

L-Glutamate (L-Glu) transporters, EAATs, are the only significant mechanism for removal of L-Glu from extracellular fluid and maintenance of non-toxic concentrations. A growing body of evidence has suggested the correlation of EAATs with synaptic transmission and a variety of central nervous system (CNS) diseases (1).

Non-steroidal anti-inflammatory drugs (NSAIDs) are major anti-inflammation drugs and their effects are attributed to the inhibition of cyclooxygenase. Although NSAIDs are reported to have diverse effects on the CNS (2, 3), their effects cannot be explained only by their anti-inflammatory effects.

In recent report, fenamates, a group of NSAIDs, modulated substrate-induced current through EAATs (4, 5), suggesting a new molecular target for NSAIDs. We therefore investigated the effects of other types of NSAIDs on EAAT1.

All procedures were in accordance with the Guiding Principles for the Care and Use of Laboratory Animals approved by The Japanese Pharmacological Society. The detailed methods for expression of EAAT1 in oocytes and electrophysiology were shown in the Supplementary Methods (available in the online version only). L-Glu was applied for 15 s with regular 30-s intervals. NSAIDs were applied from 30 s before to 5 s after the end of the application of L-Glu.

The NSAIDs were dissolved as follows: niflumic acid (NFA) (Sigma, St. Louis, MO, USA), 300 mM in DMSO; diclofenac (Wako, Osaka), 300 mM in MeOH; aspirin (Wako), 300 mM in EtOH; and indomethacin (Sigma), 100 mM in EtOH. Arachidonic acid (AA) (Calbiochem, Darmstadt, Germany) was dissolved at 100 mM in DMSO.

All data were given as the mean ± S.E.M. *P* values were obtained by statistical analysis, as noted in the figure legends.

The left traces in Fig. 1A-a illustrate inward control current produced by L-Glu (30 μM) in *Xenopus* oocytes expressing EAAT1 at −50 mV (bold line) and −120 mV (thin line). We examined the effects of a variety of NSAIDs (Fig. 1: A and B). At −50 mV, NFA (300 μM – 3 mM) inhibited the EAAT1 current dose-dependently. At −120 mV, NFA enhanced EAAT1 current and the effect was significant at 3 mM. *Xenopus* oocytes have endogenously Ca^{2+}-activated Cl^- channels (CaCC) and Ca^{2+} entry through voltage-dependent Ca^{2+} channels elicits a

*Corresponding author. kasato@nihs.go.jp
Published online in J-STAGE on January 6, 2010 (in advance)
doi: 10.1254/jphs.09260SC

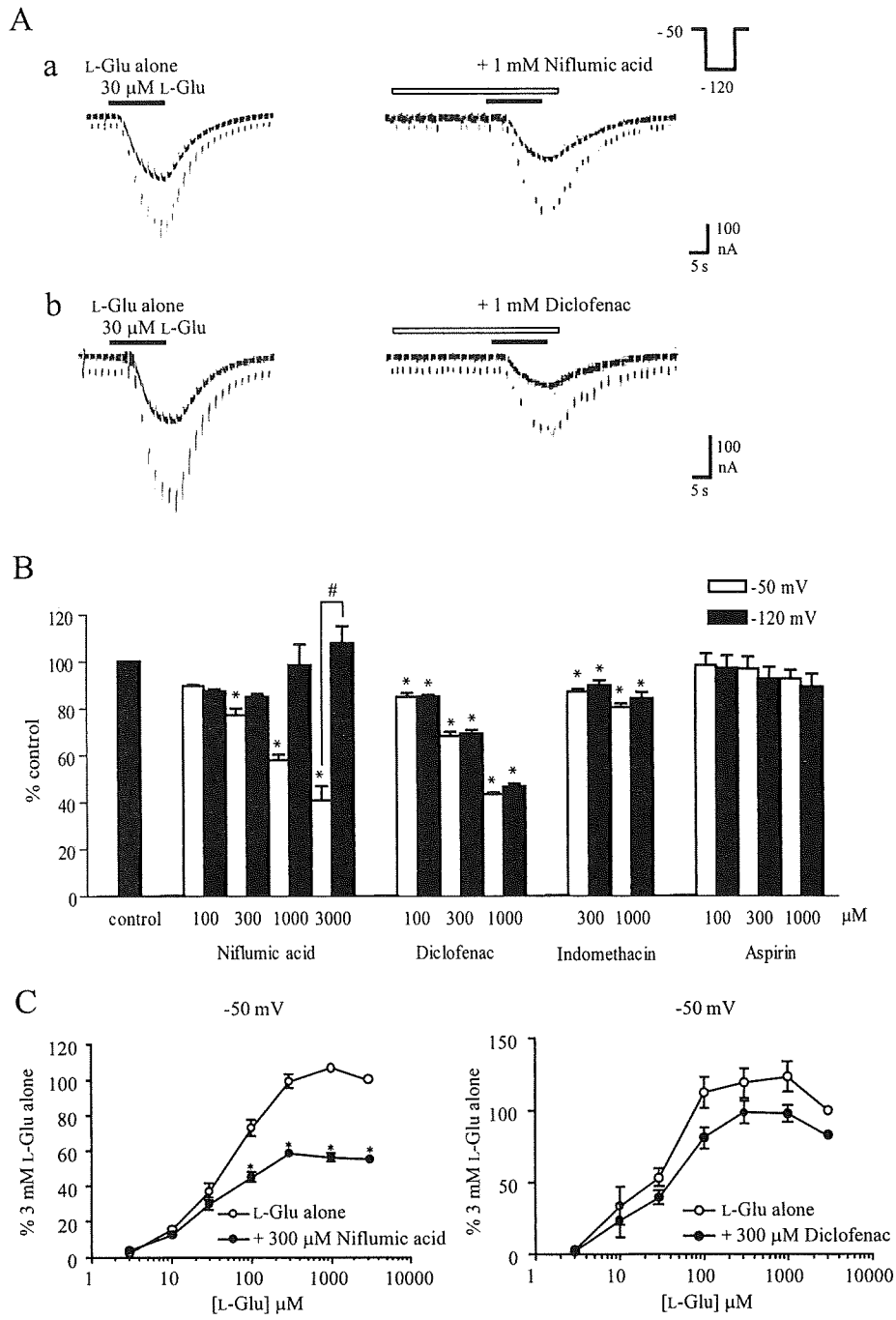

Fig. 1. Effects of NFA and diclofenac on L-Glu-induced currents in EAAT1-expressing *Xenopus* oocytes. A: The traces of L-Glu (30 μM)–induced inward currents in the presence or the absence of NFA (a) or diclofenac (b) at −50 mV (bold line) and −120 mV (thin line). The oocytes were held at −50 mV and hyperpolarized to −120 mV for 400 ms, every 2 s. B: Concentration–response relationships for various NSAIDs at −50 and −120 mV. The amplitude of EAAT1 current in the presence of the drug was normalized to that just before the application. NFA (n = 5 – 9), diclofenac (n = 5), and indomethacin (n = 5) significantly inhibited EAAT1 currents. Aspirin (n = 4) did not affect EAAT1 currents. The inhibition by NFA was always more remarkable at −50 mV than at −120 mV. $^{*}P < 0.05$ vs. the control group. $^{\#}P < 0.05$ vs. the −50 mV group. Tukey's test following ANOVA. C: Concentration–response curves of EAAT1 currents at −50 mV in the absence or the presence of NFA (n = 9) (left) or diclofenac (n = 8) (right). The currents were normalized to the maximal current induced by 3 mM L-Glu. I_{max} and $K_{0.5}$ were calculated using every concentration–response trace by fitting with the following equation: $I = I_{max}[\text{L-Glu}] / (K_{0.5} + [\text{L-Glu}])$, using Graphpad PRISM 4 for Windows. Mean I_{max} with the drug was normalized to the mean I_{max} without drug. Treatment with NFA (n = 9) and diclofenac (n = 8) resulted in a decrease in the I_{max} without affecting the $K_{0.5}$ (Student's *t*-test). $^{*}P < 0.05$ vs. the control group. Tukey's test following ANOVA.

transient outward current varied by Cl^-. Although NFA is reported to inhibit CaCC (6), the contribution of CaCC to EAAT1 current may be negligible at −50 and −120 mV according to the report. Diclofenac (100 μM − 1 mM) inhibited the EAAT1 current dose-dependently. Indomethacin (100 and 300 μM) inhibited the EAAT1 current, but the effects were even weaker. In the case of diclofenac and indomethacin, the strength of the effects at −50 and −120 mV were almost the same. Aspirin (100 μM − 1 mM) had no effects. At −50 mV, co-application of NFA with varying doses of L-Glu significantly reduced the maximal current (I_{max}) to 55.1 ± 1.8% (Fig. 1C, left). The affinity for L-Glu ($K_{0.5}$) was not affected by NFA (from 50.0 ± 5.0 to 33.9 ± 6.3 μM). Similarly, diclofenac resulted in a decrease in the I_{max} (81.7 ± 1.2%) without affecting the $K_{0.5}$ (from 27.3 ± 4.0 to 35.2 ± 6.3 μM) in a non-competitive manner (Fig. 1C, right). Although vehicle alone had no significant effect on I_{max} and $K_{0.5}$ (data not shown), the $K_{0.5}$ value for diclofenac-vehicle was smaller than that for NFA-vehicle, which might have been attributed to the slight conformational change caused by DMSO and MeOH. Taken together, these results suggest that NFA and diclofenac modulate EAAT1 via a site different from the L-Glu recognition site.

AA is known to decrease EAAT1 current in a noncompetitive manner (7). Therefore, we compared the effects of NFA and diclofenac when co-applied with AA. The doses used for NFA and diclofenac were determined so as to obtain the equivalent effects and not to reach maximum effects (Fig. S1) (Supplementary Figure: available in the online version only). NFA and AA have an almost additive effect (Fig. 2A). Diclofenac and AA did not show an additive effect (Fig. 2B). The enhancement by AA of diclofenac's effect was significantly weaker than that of NFA's effect (Fig. 2C). These results imply that NFA and diclofenac interact with EAAT1 in different manners.

Figure 3A shows representative current–voltage curves for the EAAT1 currents in the presence or in the absence of NFA. The current value in the presence of NFA alone has been subtracted from that in the presence of NFA and L-Glu. NFA produced a significant leftward shift of reversal potential (E_{rev}) (from 28.9 ± 5.1 to 5.2 ± 5.7 mV). At the potentials more negative than −100 mV, NFA increased the current amplitude. The influence of NFA on the current amplitude was voltage-dependent (Fig. 3B). Diclofenac inhibited the current amplitude to the same extent at all negative potentials and had no effects on the E_{rev} (from 33.8 ± 9.1 to 27.5 ± 6.1 mV) (Fig. 3: C and D). These results further support the implication that NFA and diclofenac interact with EAAT1 in different manners.

The differences in voltage dependency and the effects

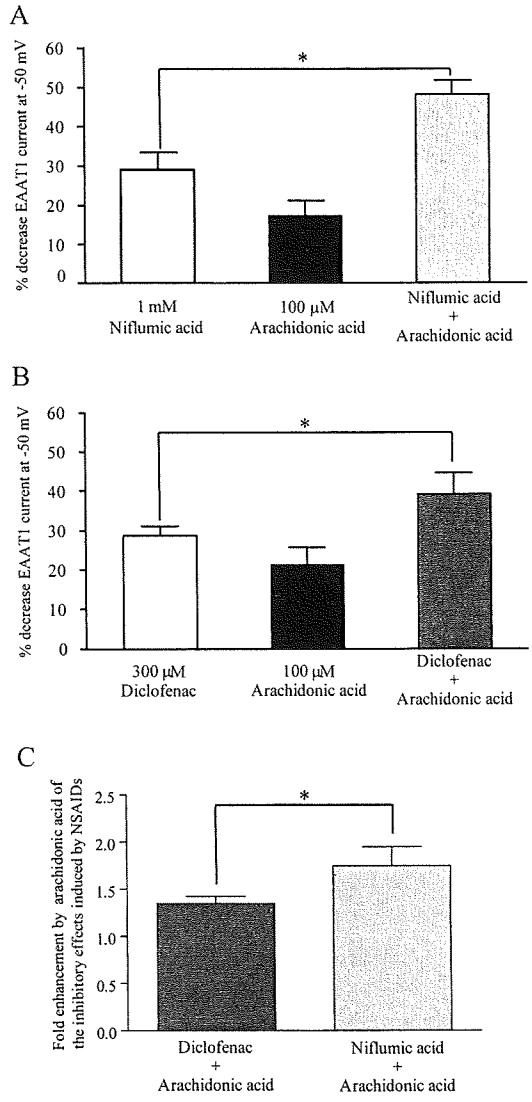

Fig. 2. AA differently influenced the effects of NFA and diclofenac. A and B: The percentage decrease was calculated by comparing the current amplitude induced by 30 μM L-Glu with drugs to that induced by L-Glu alone at −50 mV. NFA and AA have an almost additive effect (28.9 ± 4.6% decrease for NFA [1 mM], 17.4 ± 3.8% decrease for AA [100 μM], 48.3 ± 3.4% decrease for NFA + AA, n = 4). Although AA also enhanced the inhibitory effect of diclofenac, the enhancement was even weaker than that of NFA (28.7 ± 2.6% decrease for diclofenac [300 μM], 21.3 ± 4.3% decrease for AA [100 μM], 39.3 ± 4.0% decrease for diclofenac + AA, n = 5). *$P < 0.05$ vs. the NSAIDs alone group. Paired t-test. C: The fold enhancement was calculated by comparing the percentage decrease by NSAIDs to that by NSAIDs with AA at −50 mV. The enhancement by AA of diclofenac's effects was significantly weaker than that of NFA's effect (1.7 ± 0.2 vs. 1.3 ± 0.1 fold; *$P < 0.05$, Student's t-test).

on E_{rev} suggest that NFA and diclofenac regulate EAAT1 via different mechanisms. The EAAT1 currents are the net result of charge movements from amino acid (aa) and ion cotransport (Na^+ / H^+ / K^+) (I_{aa}) and the ligand-gated Cl^- conductance (I_{Cl}) (8). NFA has been reported to en-

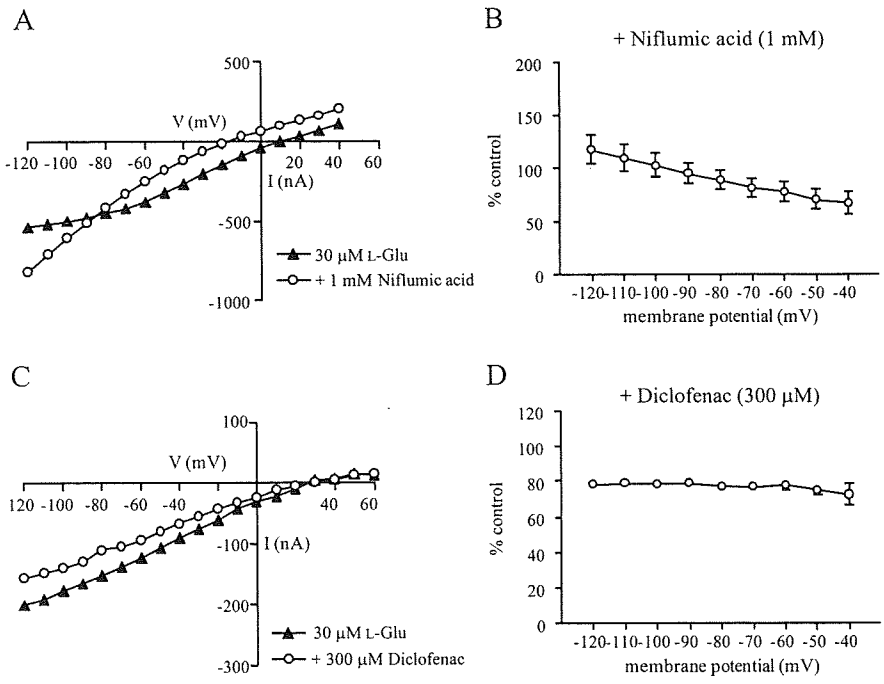

Fig. 3. The effect of NFA is voltage-dependent. A and C: Representative current–voltage relations for 30 μM L-Glu in the presence or the absence of 1 mM NFA (A) and 300 μM diclofenac (C). The current–voltage relationships were obtained with a holding potential of −50 mV and implementing 400-ms voltage jumps in 10-mV increments over the range from −120 to +60 mV. In the control, current values at steady-state have been subtracted from that in the presence of L-Glu. In the drug (NFA or diclofenac)–treated group, the current value in the presence of drug alone has been subtracted from that in the presence of the drug and L-Glu. NFA (n = 10) produced a leftward shift of E_{rev} ($P < 0.05$), whereas diclofenac (n = 4) had no effect (paired t-test). B and D: The relationship between the effects and the holding potential. The current in the presence of these drugs was normalized to that obtained just before the application. The effect of NFA (n = 10) was voltage-dependent. Diclofenac (n = 5) inhibited the current amplitude to the same extent at all negative potentials.

hance the L-Glu-induced EAAT4 current by activating an uncoupled H^+ conductance (5). In our preliminary data, NFA did not cause a modulation in the rate of I_{aa} and I_{Cl}, but rather modulates an uncoupled H^+ conductance of EAAT1 (unpublished observation), which may be related to the effect of NFA obtained in our study. In contrast, diclofenac altered only the current amplitude but not the E_{rev}. E_{rev} for the net current depends on the relative magnitude of I_{aa} and I_{Cl} (8). Diclofenac might have affected both I_{aa} and I_{Cl} so as not to change E_{rev}. The mechanism for the effects of diclofenac needs further investigation.

In our study, the influences on EAAT1 currents were caused by NFA, diclofenac, and indomethacin but not by aspirin. Mefenamic acid, diclofenac, and indomethacin are known to induce reproducible symptoms in patients with affective disorder (9). Aspirin has not been reported to have such side defects to date. If you take into account that GLAST (rodent EAAT1)–deficient mice showed phenotypic abnormalities related to schizophrenia (10), our results suggest that the psychiatric side effects of some NSAIDs have correlation with their effects on L-Glu transporters. Because NSAIDs have high affinity with the plasma protein, their brain delivery is restricted by the blood brain barrier (11). For example, the concentration of enantiomers of ibuprofen in cerebrospinal fluid is less than 1.5 μM after therapeutic application (12). Based on these data, the effective concentrations of NFA and diclofenac in our study are higher than that expected for therapeutic application. Habjan et al. recently indicated that EAAT1 current was inhibited by NFA. The extent of the effects was application time–dependent and partially irreversible (4), raising the possibility that NFA and diclofenac modulate EAAT1 after long-term administration.

NSAIDs are widely used for patients with inflammation, fever, and pain. Our results may help understanding the mechanisms of side effects caused by some NSAIDs.

Acknowledgments

We thank Dr. Yasuda-Kamatani and Dr. Shimamoto for providing the cDNA of EAAT1 and Dr. Nakagawa and Dr. Shigeri for helpful suggestions. This work was partly supported by a Grant-in-Aid for Young Scientists from MEXT, Japan (KAKENHI 18700373, 21700422); a Grant for Research on Publicly Essential Drugs and Medical Devices from JHSF; and a Health and Labor Science Research Grant for Research on Risks of Chemicals from MHLW, Japan, awarded to K.S.

References

1 Beart PM, O'Shea RD. Transporters for L-glutamate: an update on their molecular pharmacology and pathological involvement. Br J Pharmacol. 2007;150:5–17.
2 Wahner AD, Bronstein JM, Bordelon YM, Ritz B. Nonsteroidal anti-inflammatory drugs may protect against Parkinson disease. Neurology. 2007;69:1836–1842.
3 Browning CH. Nonsteroidal anti-inflammatory drugs and severe psychiatric side effects. Int J Psychiatry Med. 1996;26:25–34.
4 Habjan S, Vandenberg RJ. Modulation of glutamate and glycine